ACS NANO

www.acsnano.org

ARTICLE

On-Site Serine Delivery Drives Fermentation Pathway Reprogramming to Reverse Intracellular *Staphylococcus aureus* Persistence

Diandian Huang,[#] Xiaoxu Kang,[#] Zibo Yin, Dongdong Zhao, Yuchen Ning, Huan Liu, Feng Li, Wensheng Xie, Guofeng Li,* and Xing Wang*

Cite This: https://doi.org/10.1021/acsnano.5c06864

Read Online

ACCESS | Metrics & More | Article Recommendations | Supporting Information

ABSTRACT: **Intracellular *Staphylococcus aureus* bacteria that survive high-dose antibiotic treatment are recognized as persisters, serving as reservoirs for recurrent infections. While enhancing bacterial metabolism has restored antibiotic efficacy against planktonic persisters, it is ineffective against intracellular forms due to host-imposed nutrient deprivation. To address this, we developed FAlsBm@Rif, a poly(amino acid)-based nanodrug designed to sensitize intracellular persisters to antibiotics via on-site serine delivery. FAlsBm@Rif is constructed by encapsulating rifampicin in serine- and mannose-functionalized copolymers, FAlsBm. Upon uptake of FAlsBm@Rif by macrophages through mannose-mediated endocytosis, the mannose ligand dissociates within the host cell, exposing phenylboronic acid groups to the nanodrug. This enables FAlsBm@Rif to specifically target the peptidoglycan of intracellular persisters. In this way, FAlsBm@Rif employs a cascade-targeting mechanism to precisely navigate both host cells and intracellular *Staphylococcus aureus* persisters, ensuring the localized release of serine and rifampicin at bacterial loci, thus counteracting host-imposed nutrient deprivation. On-site serine delivery shifts persisters to a fermentation pathway under host-induced stress, boosting ATP production and membrane potential. This metabolic shift reverses persistence by alleviating the stringent response and reducing cell wall stress. Consequently, FAlsBm@Rif eradicated 99.78% of intracellular persisters in vivo, significantly outperforming Rif alone (63.41%). This strategy offers a promising approach to combating intracellular persisters.**

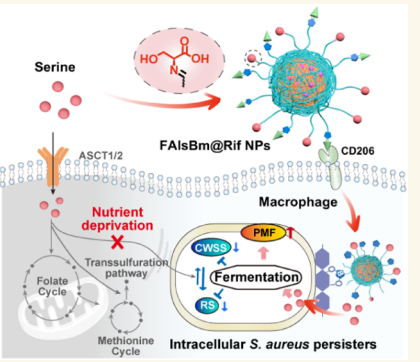

KEYWORDS: *poly(amino acid)-based nanodrug, intracellular Staphylococcus aureus persisters, on-site serine delivery, fermentation reprogramming, sensitizing antibiotic treatment*

INTRODUCTION

Intracellular survival of pathogens enables them to multiply inside host cells and manipulate their biology,[1−3] which is widely recognized as a major factor in the recurrence of various infections, including osteomyelitis, endocarditis, pneumonia, and sepsis.[4−6] *Staphylococcus aureus* (*S. aureus*), one of the most opportunistic pathogens infecting humans,[7] is increasingly recognized as an intracellular pathogen that invades, hides, and settles in various types of host cells. The intracellular niche boosts the survival of *S. aureus*. Treatment often requires prolonged and intensive antibiotic therapy;[8] however, intracellular *S. aureus* has been shown to become less responsive to antibiotic action even in the absence of genetically detectable antimicrobial resistance, leading to frequent treatment failures.[9] The high rates of antibiotic treatment failure are surprising and suggest a mechanism beyond antibiotic resistance.[10]

S. aureus within host cells surviving antibiotic treatment are classified as persisters.[11] Intracellular *S. aureus* persisters exist in a nongrowing state, which confers their tolerance to lethal concentrations of multiple antibiotic classes targeting unrelated pathways,[12] while they can rapidly revert to a normal metabolic state upon antibiotic removal without any genetic changes.[13,14] Therefore, achieving effective eradication of these intracellular

Received: April 24, 2025
Revised: July 1, 2025
Accepted: July 3, 2025

Scheme 1. Schematic Illustration of Intracellular *S. aureus* Persister Killing by FAlsBm@Rif NPs through On-Site Ser and Rif Delivery[a]

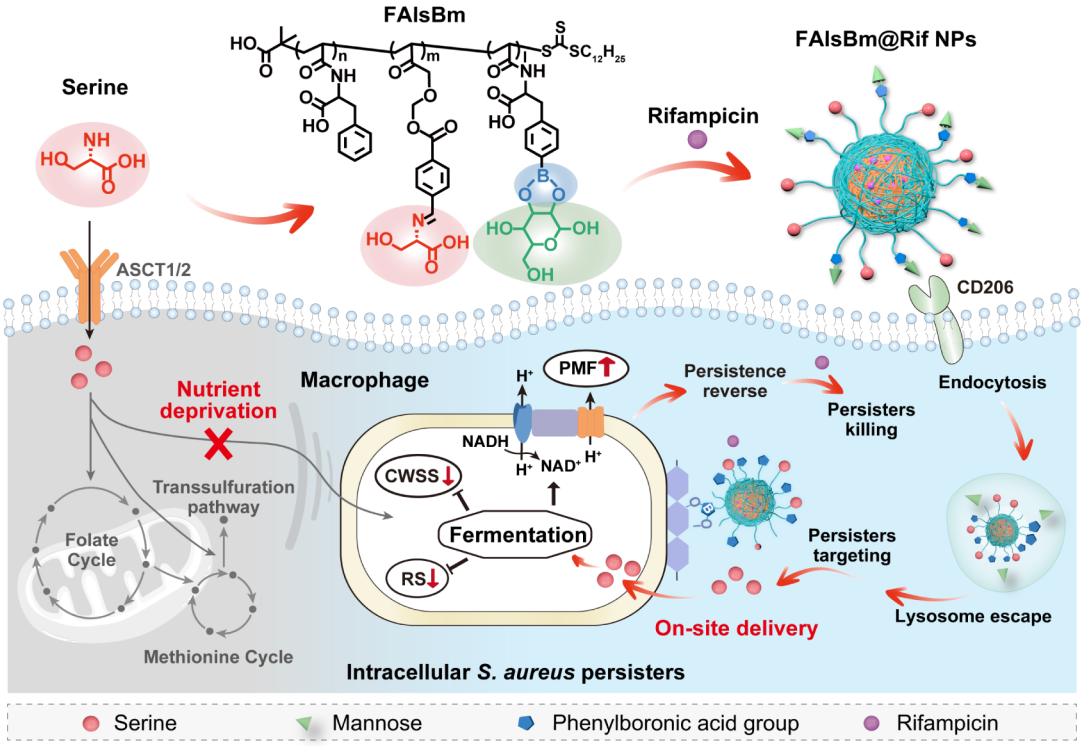

[a]To overcome host cell membrane barriers and nutrient deprivation, FAlsBm@Rif NPs are engineered to sequentially target host cells and intracellular *S.aureus* persisters. The NPs enter macrophages via Man-mediated endocytosis, while phenylboronic acid groups facilitate lysosomal escape and anchor the NPs to the peptidoglycan on persister surfaces through an ester-exchange reaction. This on-site delivery results in the release of Ser and Rif at the persister site. The released Ser reprograms the fermentation pathway, reversing *S.aureus* persistence and sensitizing the persisters to antibiotic treatment.

S. aureus persisters presents a significant challenge. To date, enhancing the susceptibility of planktonic persisters to antibiotic killing by restoring bacterial metabolism has been widely studied.[15−17] Nutritional supplementation, such as sugars and amino acids, can boost bacterial activity and revert the persistent state, thereby sensitizing persisters to antibiotics.[15,16,18] However, these strategies are difficult to apply in treating intracellular bacterial persisters. The bacterial cellular uptake of nutritional supplementation is limited by the metabolic flow of host cells.[19] The homeostasis of these nutrients within the host cell reduces their effectiveness in modulating intracellular *S. aureus* persisters.[12] Moreover, restricted drug uptake and the acidic, hydrolytic environment within phagolysosomes lead to low intracellular concentrations and diminished antibacterial activity of antibiotics.[20,21] Thus, the contribution of nutritional supplementation in sensitizing intracellular *S. aureus* persisters to antibiotic killing is significantly compromised.

In this study, we proposed an on-site delivery strategy to sensitize antibiotic killing of intracellular *S. aureus* persisters by amino acid-induced metabolic enhancement (Scheme 1). Poly(amino acid)-based nanodrugs were engineered by encapsulating antibiotics within serine (Ser)- and mannose (Man)-functionalized copolymers FAlsBm. Rifampicin (Rif), a potent bactericidal agent against intracellular bacteria, was selected as the model antibiotic. The resulting nanoparticles (NPs), FAlsBm@Rif NPs, employed a cascade-targeting strategy to sequentially navigate host cells and *S. aureus* persisters, delivering antibiotics and amino acids directly to intracellular bacterial loci. This strategy overcame host cell membrane barriers and counteracted nutrient depletion within the host, enabling targeted actions toward intracellular persisters. Upon delivery, Ser was metabolized within the bacteria, converting to pyruvate through dehydration and deamination, which then activated the fermentation pathway of intracellular *S. aureus* persisters. This metabolic activation resulted in enhanced adenosine triphosphate (ATP) production and the proton motive force (PMF). The subsequent metabolic reprogramming reversed the persistence of intracellular *S.aureus*, accompanied by reduced stringent response (SR) and bacterial cell wall stress stimulation (CWSS). Consequently, the killing efficacy of codelivered Rif against intracellular persisters was significantly enhanced, achieving a 99.78% killing rate of intracellular *S. aureus* persisters in vivo, significantly outperforming Rif (63.41%) alone. Together, this work provides insights into reversing bacterial persistence and offers a new approach for eliminating intracellularly persistent bacteria.

RESULTS AND DISCUSSION

Ser Supplementation Boosts Antibiotic Killing of Planktonic Persisters, but Not Intracellular Ones. Planktonic persisters were generated by exposing methicillin-resistant *S. aureus* (MRSA, clinically isolated from a hospital) cultures to 50 μg/mL vancomycin (Van) for 8 h during the stationary phase.[22,23] This treatment selectively eliminated

https://doi.org/10.1021/acsnano.5c06864
ACS Nano XXXX, XXX, XXX−XXX

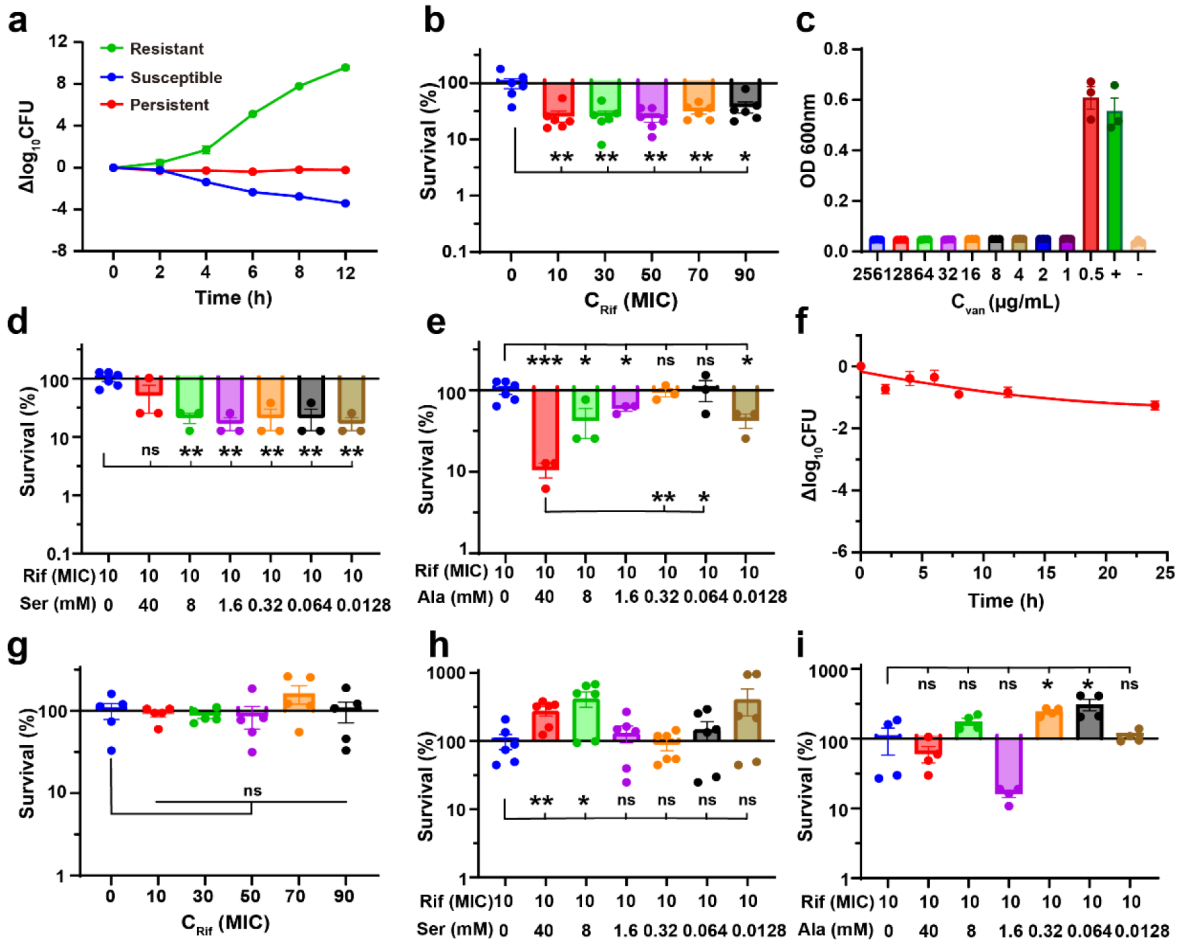

Figure 1. Establishment and evaluation of persistent *S. aureus* and their survivals upon antibiotic and amino acid treatments. a) Time-kill curves of planktonic bacterial subpopulations. Susceptible, persistent, and resistant subpopulations were exposed to 50× MIC of Van, Van, and amoxicillin (Amo), respectively (n = 3). b) Survival of planktonic persisters following Rif exposure (n = 6). c) MIC of *S. aureus* recovered from a persistent state (n = 3). The killing effects of Rif in combination with d) Ser (n = 3) and e) Ala (n = 3) against planktonic persisters. f) Time-kill curves of intracellular persisters exposed into 50× MIC of Van (n = 5). Survival of the intracellular persisters exposed to g) Rif (n = 5), h) Rif plus Ser (n = 6), and i) Rif plus Ala (n = 4). The cells used in the experiment were Raw264.7 macrophage. Data are means ± SEM of independent experiments. Source data are provided as a Source Data file. Statistical significance was determined by unpaired t test (two-tailed). **** $p < 0.0001$, *** $p < 0.001$, ** $p < 0.01$, * $p < 0.05$, ns $p > 0.05$.

antibiotic-susceptible cells, enriching a surviving subpopulation of persistent bacteria. To further distinguish persisters from other subpopulations, a time-kill kinetics assay was conducted in the presence of antibiotics (Figure 1a). The susceptible subpopulations exhibited a classic killing profile with a rapid decline in colony counts, while the resistant subpopulations continued to proliferate throughout the monitoring period. In contrast, persisters were subpopulations that transiently adopted a nongrowing, tolerant phenotype.[24,25] Thus, persister cells showed a markedly different kinetic profile, with the ability to withstand high-dose antibiotics accompanied by minimal mortality (Figures 1a and S1). Furthermore, the persisters maintained a stable undiminished population regardless of the lethal concentration of Rif (Figures 1b and S2). However, when re-exposed to the fresh medium without antibiotics, the persisters reverted to a susceptible phenotype, displaying the same minimum inhibitory concentration (MIC) value as the susceptible bacteria (Figure 1c).

It has been reported that exogenous amino acids could enhance the antibiotic uptake by increasing the TCA cycle flux, thereby restoring antibiotic killing.[26,27] Ser and alanine (Ala) were used to enhance the susceptibility of antibiotics against planktonic persisters. As shown in Figures 1d and S3, Ser, across a wide range of concentrations (0.0128−40 mM), exhibited a reinforced performance, while Ala demonstrated a concentration-dependent killing effect (Figures 1e and S4). Specifically, Ser and Ala increased the antibiotic killing of planktonic persisters to 83.0% and 89.4%, respectively.

Intracellular bacteria that survive antibiotic treatment within host cells have been shown to exhibit a persistent phenotype, as demonstrated by Peyrusson and colleagues.[12] To generate intracellular persisters, we exposed intracellular MRSA to 50× MIC of Van for 24 h. The resulting intracellular persisters remained in a nongrowing and slowly killing state upon exposure to 50× MIC of Van, exhibiting a time-kill kinetic profile similar to that of planktonic persisters (Figures 1f and S5). Moreover, increasing the antibiotic did not lead to enhanced killing of intracellular persisters (Figures 1g and S6), suggesting that intracellular persisters were more adept at evading antibiotic clearance.

To determine whether exogenous amino acids could reinforce the antibiotic killing of intracellular persisters, the combinations of Ser/Ala and Rif were tested. However, these combinations failed to treat intracellular persisters, which

https://doi.org/10.1021/acsnano.5c06864
ACS Nano XXXX, XXX, XXX−XXX

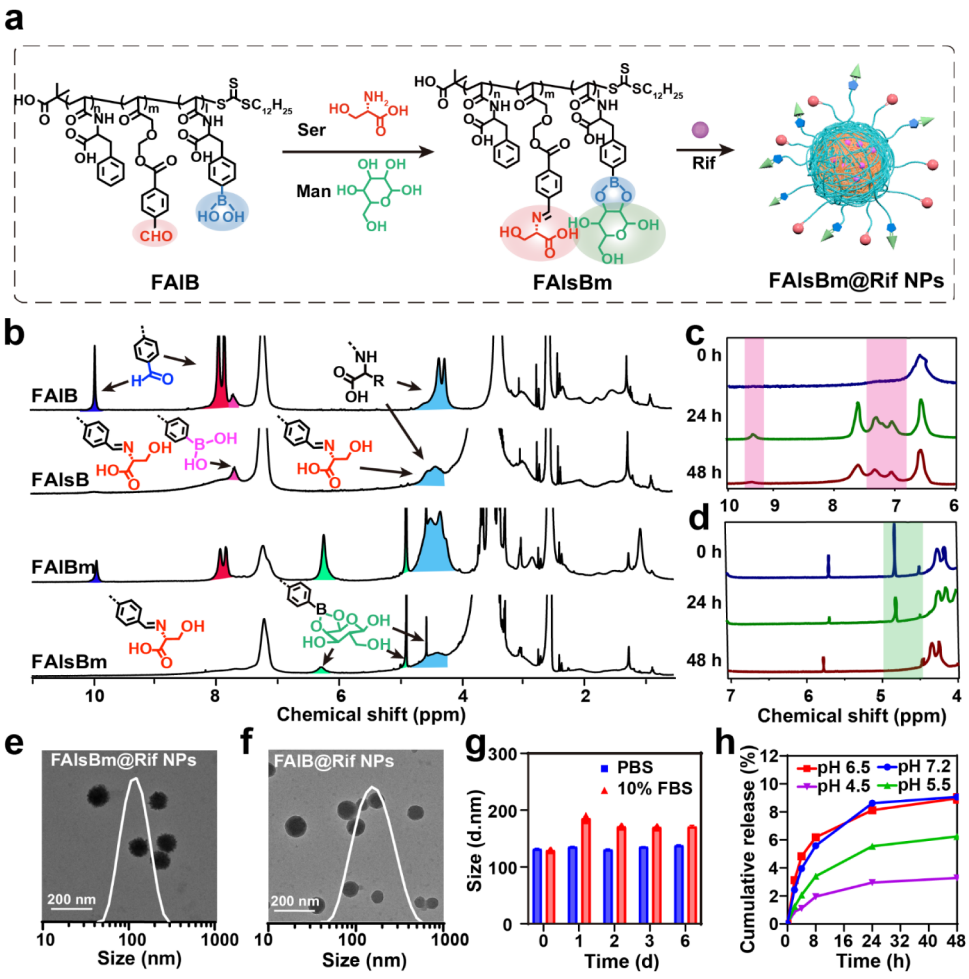

Figure 2. Construction and characterization of FAlsBm NPs. a) Schematic illustration of FAlsBm@Rif NPs. b) ^{1}H NMR spectra (400 Hz, DMSO-*d6*) of the FAlsBm polymer and its derivatives. Release of c) Ser and d) Man from FAlsB and FAlBm triggered by acidic pH 5.5. The labeled regions in (c) and (d) are the peaks of the re-exposed benzaldehyde groups and the Man groups, respectively. TEM images and size distribution of e) FAlsBm@Rif NPs and f) FAlB@Rif NPs. g) Stability of FAlsBm@Rif NPs in PBS and 10% FBS over 6 days (n = 3). h) Release profiles of Rif from FAlsBm@Rif NPs at different pH values (n = 3). Data are means ± SEM (g,h) or representative results (b−f) of independent experiments. (e−h) Source data are provided as a Source Data file.

displayed volatile yet high survival patterns in the presence of Ser/Ala plus Rif (Figures 1h,i, S7, and S8). These results supported the idea that metabolic adaptations occurred in host cells during acute bacterial infection. While intracellular persisters attempt to deprive nutrients from the host cell, the host cell mounts metabolic countermeasures to resist nutrient theft.[28] Consequently, the supplementation of Ser/Ala was insufficient to enhance the killing effect of Rif on intracellular persisters.

FAlsBm Design for Targeted Delivery of Amino Acid and Antibiotics to Intracellular Bacteria Loci. Accordingly, we hypothesized that on-site delivery of amino acids to the bacterial loci could boost the uptake and metabolism of intracellular persisters while minimizing nutrient limitation in host cells, thereby enhancing antibiotic killing of the persisters. To test this, we designed a drug delivery system that enabled the targeted delivery of both amino acids and antibiotics to intracellular *S. aureus* persisters. As illustrated in Figure 2a, a triblock copolymer poly(*N*-acryloyl phenylalanine)-*b*-poly(2-((4-formylbenzyl)oxy) acrylic acid ethyl ester)-*b*-poly((S)-2-acrylamido-3-(4-boronphenyl) propionic acid) (denoted as FAlB) was synthesized via a photoinduced electron/energy transfer-reversible addition−fragmentation chain-transfer (PET-RAFT) polymerization technique (Figures S9 and 10). The poly(*N*-acryloyl phenylalanine) (PF) segment served as the hydrophobic core for loading the antibiotic Rif. The poly(2-((4-formylbenzyl)oxy) acrylic acid ethyl ester) (PAl) segment, containing aldehyde groups, was designed to react with amino acids via a Schiff-base reaction. Under acidic conditions, the Schiff-base bond could be cleaved, enabling the release of amino acids. Additionally, the poly((S)-2-acrylamido-3-(4-boronphenyl) propionic acid) (PB) segment was incorporated to facilitate reaction with Man by means of an esterification reaction. Man was chosen to promote cellular uptake via the Man-acceptors on macrophage surfaces.[29,30] After cellular uptake, the PB segment could then anchor to the peptidoglycan of intracellular *S. aureus* persisters through an ester-exchange reaction.[31,32] The molecular weight of FAlB was determined to be 19 200 g/mol, with the composition ratio of PF, PAl, and PB being 30:40:20, respectively (Figure S11). Next, Ser and Man were sequentially grafted to FAlB via a Schiff-base reaction and an esterification reaction, respectively. The specific signal peaks corresponding to Ser and Man were clearly observed in the ^{1}H NMR spectra of the synthesized FAlsBm (Figures 2b and S12). The mole ratio of FAlB, Ser, and Man in FAlsBm was 1:40:16. The ^{1}H NMR spectra further

https://doi.org/10.1021/acsnano.5c06864
ACS Nano XXXX, XXX, XXX−XXX

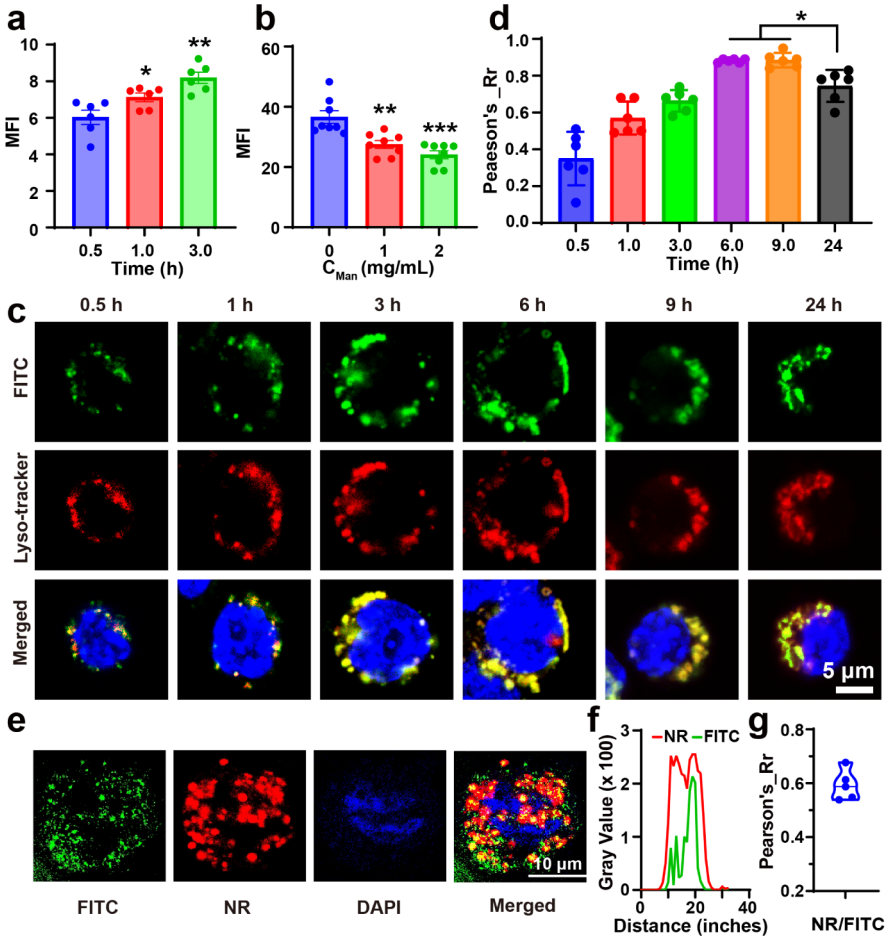

Figure 3. Targeting properties of FAlsBm NPs toward macrophages and intracellular *S. aureus*. a) Time-dependent cellular uptake of FAlsBm@NR NPs (n = 6). b) Mean fluorescence intensity (MFI) of internalized Nile Red-loaded FAlsBm NPs (denoted as FAlsBm@NR NPs) in the presence of varying concentrations of the competitive inhibitor Man (n = 8). c) Colocalization confocal images of FAlsBm@FITC and lysosomes at different coincubation times (n = 9, red: Lyso-Tracker Red; green: FITC; blue: DAPI). d) Corresponding Pearson's correlation coefficient for the colocalization in (c). e) Colocalization confocal images of intracellular FITC-labeled *S. aureus* and FAlsBm@NR (red: Nile Red; green: FITC; blue: DAPI). f) Colocalization fluorescence intensity profiles and g) colocalization Pearson's_Rr between FITC-labeled *S. aureus* and FAlsBm@NR corresponding to (e) (n = 5). The cells used in the experiment were Raw264.7 macrophage. Data are means ± SEM (a,b,d) or representatives results (c,e,f,g) of independent experiments. (a,b,d,f,g) Source data are provided as a Source Data file. Statistical significance was determined by unpaired t test (two-tailed). **** $p < 0.0001$, *** $p < 0.001$, ** $p < 0.01$, * $p < 0.05$, ns $p > 0.05$.

confirmed that Ser and Man could be released from FAlsBm under acidic conditions (Figure 2c,d). At pH 5.5, 57% of Ser was released after 24 h, increasing to 92% after 48 h (Figure S13), while 87.5% of Man was released after 24 h, reaching 90.0% after 48 h (Figure S14).

FAlsBm was then used to encapsulate Rif in a dimethyl sulfoxide (DMSO)/water (1/9, v/v) mixed solvent system. The blank FAlsBm NPs exhibited a normal distribution of particle sizes with an average diameter of 124.7 nm and a polydispersity index (PDI) of 0.161 (Figure S15). Upon encapsulation of Rif, the average particle size of FAlsBm@Rif NPs decreased to 108.8 nm, with a PDI of 0.122 (Figures 2e and S15). As control NPs, FAIB@Rif NPs without Ser and Man modifications were prepared by following the same procedure. The resulting NPs exhibited a spherical morphology with an average particle size of about 157 nm and a PDI of 0.167 (Figure 2f). FAlsBm@Rif NPs demonstrated stability in PBS or 10% FBS for 6 days, showing no significant changes in particle size (Figure 2g). The Rif loading efficacy was approximately 20%, and FAlsBm@Rif NPs displayed a sustained Rif release profile (Figure 2h). At 48 h, only ~8% Rif was released at pH 7.2 and 6.5, while approximately ~6% and ~3.2% were released at pH 5.5 and 4.5, respectively.

The targeting properties of FAlsBm NPs toward macrophages and intracellular *S. aureus* were investigated. FAlsBm NPs exhibited time-dependent cellular uptake, which was significantly inhibited in the presence of Man (Figures 3a,b and S16), indicating Man-mediated endocytosis of FAlsBm NPs in macrophages. After endocytosis, fluorescein isothiocyanate-loaded FAlsBm NPs (denoted as FAlsBm@FITC NPs) with green fluorescence accumulated in the lysosomes of macrophages within the first 3 h. With prolonged incubation, the phenylboronic acid groups in FAlsBm@FITC NPs interacted with lysosomal membrane proteins, triggering the transportation of the FAlsBm@FITC NPs from lysosomes to the cytoplasm of macrophages (Figures 3c,d and S17). This property is crucial for the intracellular bacterial targeting of FAlsBm NPs. Additionally, due to the abundant peptidoglycans on the surface of *S.aureus*, the phenylboronic acid groups in FAlsBm@FICT NPs displayed higher affinity for intra-

https://doi.org/10.1021/acsnano.5c06864
ACS Nano XXXX, XXX, XXX−XXX

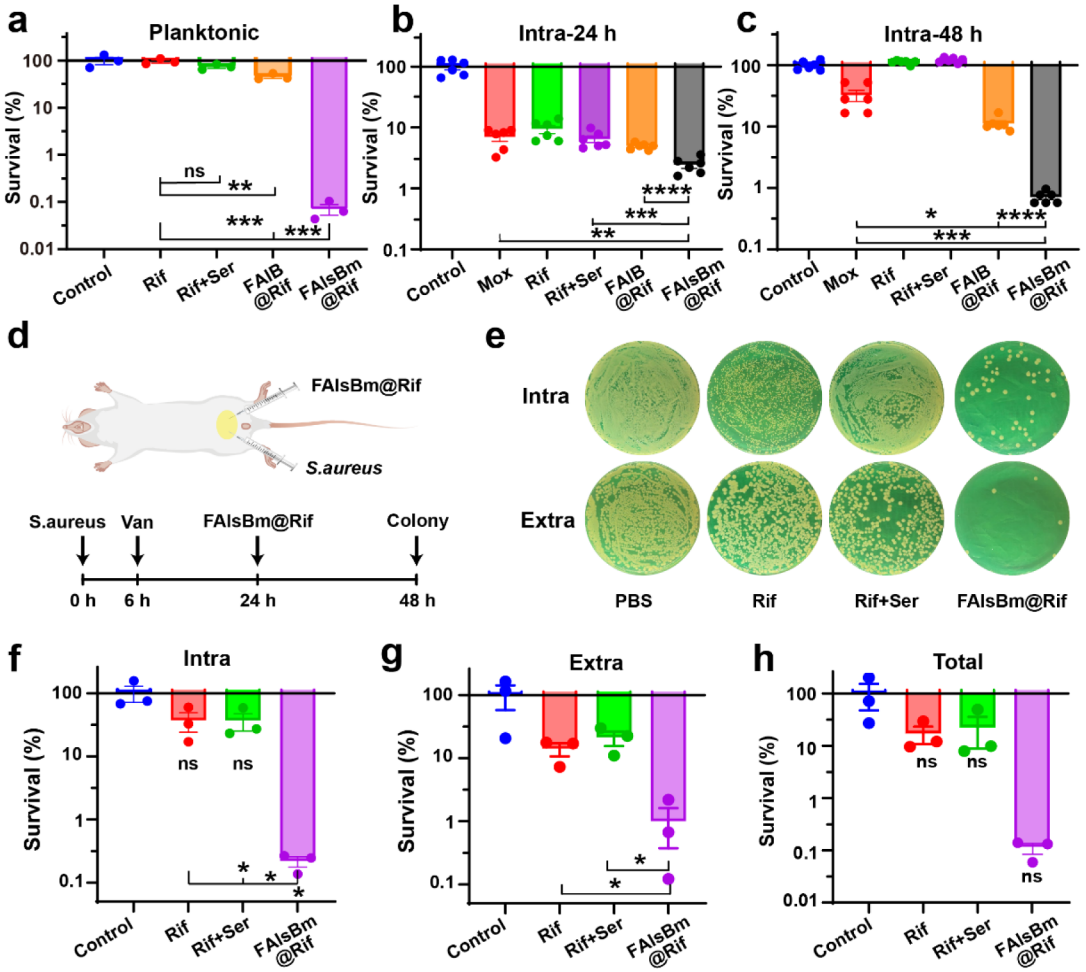

Figure 4. Killing effect of FAlsBm@Rif NPs against intracellular persisters. Percent survival of a) planktonic persisters (n = 3) and intracellular persisters after b) 24 h (n = 6) and c) 48 h (n = 6) of coincubation with FAlsBm@Rif NPs or antibiotics. d) Schematic representation of the *S. aureus* persister-induced peritonitis model. A single Rif dose (10 mg/kg) was used for antibacterial assays. e) Representative images of bacterial burden and CFU counts for f) intracellular, g) extracellular, and h) total persisters 24 h posttreatments (n = 3). The cells used in the experiment were Raw264.7 macrophage. Data are means ± SEM (a,b,c,f,g,h) or representatives results (e) of independent experiments. (a,b,c,f,g,h) Source data are provided as a Source Data file. Statistical significance was determined by unpaired t test (two-tailed). **** $p < 0.0001$, *** $p < 0.001$, ** $p < 0.01$, * $p < 0.05$, ns $p > 0.05$.

cellular *S.aureus*, specifically anchoring to the bacterial surface.[31,33] As shown in Figure 3e,f, the red fluorescence signal of FAlsBm@NR NPs coincided with the green fluorescence of FITC-labeled *S.aureus*, resulting in overlapping fluorescence upon merging (Figure 3e,f). The Pearson correlation coefficient value reached up to 59.27% (Figure 3g), indicating a good colocalization between FAlsBm NPs and intracellular *S.aureus*. These results demonstrated the potential of FAlsBm NPs for on-site delivery of Ser and Rif to targets in intracellular *S. aureus* loci.

On-Site Ser Delivery by FAlsBm@Rif NPs Enhances Rif Killing of Intracellular Persisters. Subsequently, the killing effect of FAlsBm@Rif NPs on the persisters was investigated. The combination of Ser (3.25 μg/mL) and Rif (0.7 μg/mL), at doses equivalent to those in FAlsBm@Rif NPs, was included as a control group for comparison. Consistent with previous results, the combination of Ser and Rif showed a trend toward enhanced killing of planktonic persisters compared to Rif alone (p = 0.0793, ns; Figures 4a and S18). FAlB@Rif NPs, which were loaded with Rif but lacked Ser and Man, also demonstrated a stronger killing effect (54.47%) against planktonic persisters compared to Rif (p = 0.0044, **) or Ser plus Rif (p = 0.0134, *). This suggested that the targeting effect of FAlB@Rif NPs might increase Rif uptake of intracellular persisters. Interestingly, FAlsBm@Rif NPs significantly improved the killing efficiency to 99.93% (p = 0.0002, ***), with the survival rate of persisters decreased by 1,050-fold compared to the combination of Ser and Rif. This enhanced effect could be attributed to the on-site delivery of Ser by FAlsBm@Rif NPs, which likely activated the intracellular persisters and subsequently enhanced the Rif killing effect against the persisters. Notably, Man as a sugar (a carbon source) would also be released when treating persisters. However, Ser plus Rif with or without Man exhibited similar bactericidal activity (Figure S19).

Inspired by these results, FAlsBm@Rif NPs were then used to treat intracellular persisters. After 24 h of incubation, Rif reduced the persister counts compared to the untreated group (Figures 4b and S20). Ser plus Rif showed a slight enhancement in killing intracellular persisters (93.54%) compared to Rif alone (90.64%, p = 0.0994, ns), while the combination failed to sustain efficacy after 48 h (Figures 4c and S21). Moxifloxacin (Mox), a fluoroquinolone known to enhance the killing of dormant and persistent bacteria, was

https://doi.org/10.1021/acsnano.5c06864
ACS Nano XXXX, XXX, XXX−XXX

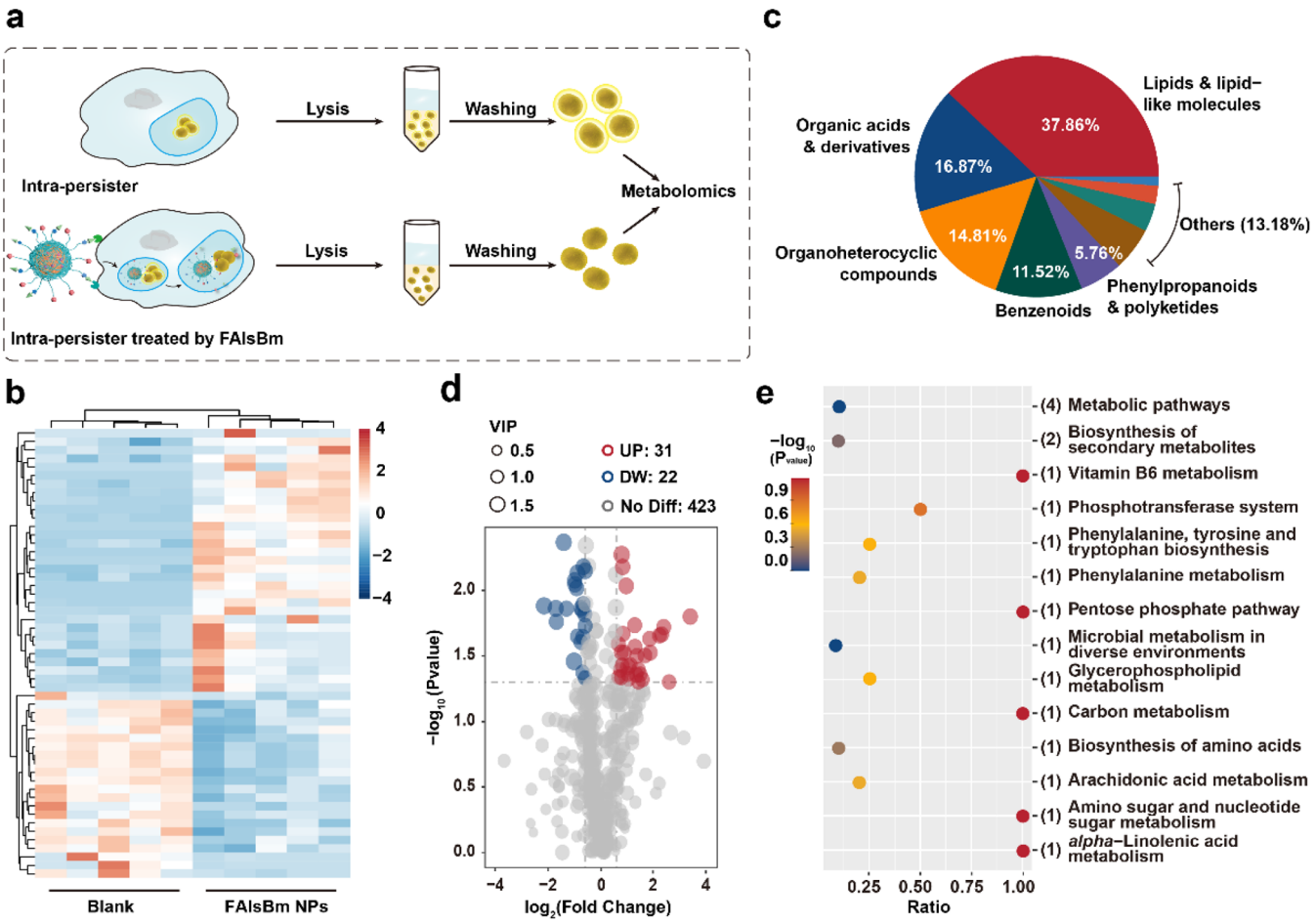

Figure 5. Metabolomics analysis of intracellular persisters treated with or without FAlsBm NPs. a) Schematic representation of the collection process for intracellular persisters used in metabolomics analysis. b) Heatmap showing hierarchical clustering of differential metabolites in intracellular persisters treated with or without FAlsBm NPs. c) Classification of identified metabolites. d) MA-plot illustrating the distribution of differential metabolites. e) KEGG pathway analysis of differential metabolites. The cells used in the experiment were Raw 264.7 macrophage. Differential metabolites were screened according to the criteria Variable Importance in the Projection (VIP) > 1.0, Fold Change (FC) > 1.5 or FC < 0.667, and *P*-value < 0.05.

used as a positive control.[9] Mox demonstrated better bactericidal activity against intracellular persisters (93.03%, $p = 0.1927$) compared to Rif and maintained stable efficacy over 48 h (67.69%, $p < 0.0001$, ****). Interestingly, FAlB@Rif NPs (88.73%) also showed superior bactericidal effects compared to Rif (~0%, $p < 0.0001$, ****) or Mox (67.69%, $p = 0.0113$, *) and the combination of Ser plus Rif (~0%, $p < 0.0001$, ****), suggesting that targeted Rif delivery via FAlB@Rif NPs could disrupt the host cell membrane barrier and facilitate Rif accumulation within intracellular persisters, thereby enhancing the killing of these persisters. Notably, FAlsBm@Rif NPs significantly reduced persister counts, exhibiting the best bactericidal performance. Approximately 99.29% of intracellular persisters were killed after 48 h of treatment with FAlsBm@Rif NPs. The residual subpopulation was 46-fold and 16-fold lower than that treated with Mox ($p = 0.0008$, ***) and FAlB@Rif NPs ($p < 0.0001$, ****). These findings strongly support that on-site delivery of Ser and Rif by FAlsBm@Rif NPs could significantly improve the susceptibility of intracellular persisters to antibiotics, which might be attributed to these NPs alleviating nutrient limitation in host cells and bolstering the utilization of Ser by intracellular persisters.

To evaluate the in vivo antimicrobial efficacy of FAlsBm@Rif NPs, an animal model of *S. aureus* persister-induced peritonitis was established (Figures 4d and S22–24). Mice were administered 1×10^8 CFUs of MRSA intraperitoneally (*I.P.*) to induce intracellular bacterial infection. Subsequently, high-dose Van (75 mg/kg) was administered *I.P.* to remove susceptible bacteria and induce the formation of a persistent subpopulation, following protocols from previous studies.[34−36] As shown in Figures 4e–h, S25, and 26, treatments with Rif alone or Rif plus Ser resulted in only mild reductions in persister counts with no significant difference compared to the untreated group. In contrast, FAlsBm@Rif NPs demonstrated superior killing efficiency against persistent bacteria in vivo. The clearance rates of FAlsBm@Rif NPs were 99.78% for intracellular bacteria and 99.01% for extracellular bacteria, significantly higher than those of Rif (intracellular bacteria: 63.41%, $p = 0.0442$, *; extracellular bacteria: 86.03%, $p = 0.0189$, *) and Rif plus Ser (intracellular bacteria: 63.73%, $p = 0.0315$, *; extracellular bacteria: 78.95%, $p = 0.0220$, *) groups. These findings highlighted that the on-site delivery of Ser and Rif by FAlsBm@Rif NPs achieved excellent eradication of intracellular persisters both in vitro and in vivo.

FAlsBm NPs Activate Intracellular Persisters via Metabolism Remodulation. To confirm the effect of

https://doi.org/10.1021/acsnano.5c06864
ACS Nano XXXX, XXX, XXX−XXX

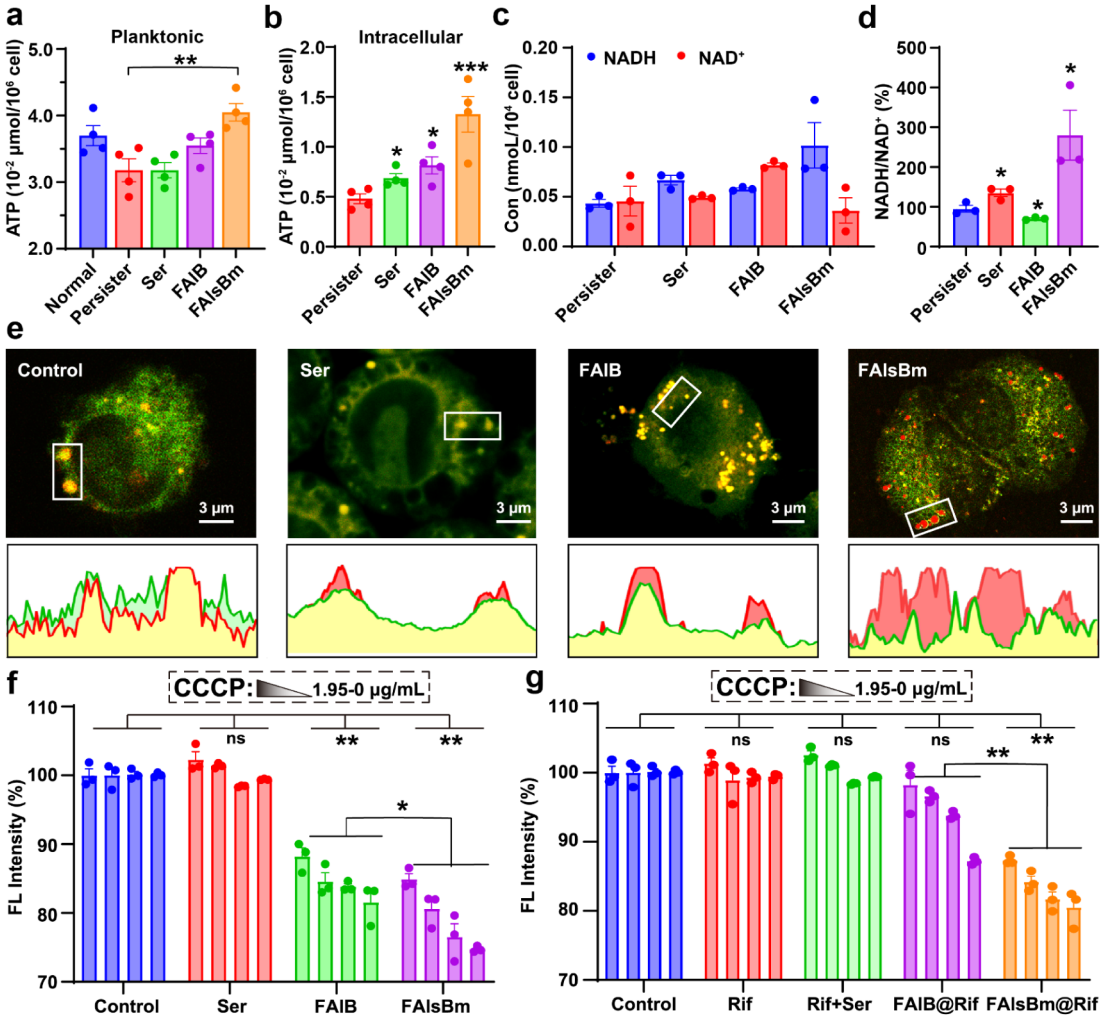

Figure 6. Switching of persistent phenotypic in intracellular bacteria through the on-site delivery of Ser by FAlsBm NPs. The ATP content in a) planktonic and b) intracellular persisters (n = 4). c) Concentration of NADH, NAD$^+$, and d) NADH/NAD$^+$ ratio in intracellular *S. aureus* persister under different treatments (n = 3). e) Confocal laser scanning microscopy (CLSM) images of intracellular persisters (1 × 10^6 CFU/mL) stained with DiOC$_2$(3) dye after 12 h of coincubation with Ser (0.325 μg/mL), FAlB NPs (1.48 μg/mL), or FAlsBm NPs (1.98 μg/mL) show that the concentration of substances in the FAlsBm@Rif NPs (Rif = 0.07 μg/mL). The insets show the green and red fluorescence. f,g) Green fluorescence intensity of planktonic persisters (1 × 10^9 CFU/mL) treated with CCCP (n = 3). The concentrations of Ser, Rif, FAlB NPs, and FAlsBm NPs are 3.25 μg/mL, 0.7 μg/mL, 14.8 μg/mL and 19.8 μg/mL, respectively. CCCP concentrations from left to right are 1.95, 0.49, 0.04, and 0 μg/mL. The cells used in the experiment were macrophage Raw264.7. Data are means ± SEM (a,−d,f,g) or representative results (e) of independent experiments. (a−g) Source data are provided as a Source Data file. Statistical significance for (f,g) and for all other data were assessed using paired and unpaired two-tailed t tests, respectively. **** p < 0.0001, *** p < 0.001, ** p < 0.01, * p < 0.05, ns p > 0.05.

FAlsBm NPs on intracellular persisters, we analyzed the metabolic activity of intracellular persisters treated with FAlsBm NPs. After 12 h of treatment with or without FAlsBm NPs, the intracellular persisters were collected by lysing the host cells and washing the samples three times with PBS (Figure 5a). Metabolomics studies were then performed on these collected persisters. Hierarchical clustering analysis revealed significant divergences and high reproducibility within each group (Figure 5b). A total of 476 metabolites were identified, which were classified into nine categories (Figures 5c and S27), including lipids and lipid-like molecules (37.86%), organic acids and their derivatives (16.87%), organic heterocyclic compounds (14.81%), benzene-type compounds (11.52%), phenylpropanes and polyketides (5.76%), organic oxides (5.76%), organic nitrogen compounds (3.70%), alkaloids and their derivatives (2.47%), and nucleic acids, nucleosides, and their analogues (1.23%). Comparative analysis revealed 53 differentially expressed metabolites between the intracellular persisters treated with and without FAlsBm NPs, with 31 metabolites upregulated and 22 metabolites downregulated (Figure 5d). KEGG pathway enrichment analysis showed that the targeted FAlsBm NPs were involved in 14 pathways (Figure 5e), including carbon metabolism, the pentose phosphate pathway, aminosugar and nucleotide sugar metabolism, vitamin B6 metabolism, and α-linolenic acid metabolism pathways. These results suggest that FAlsBm NPs might help alleviate the persistent state of intracellular persisters by modulating their metabolism.

FAlsBm NPs Enhance ATP and PMF Generation in Intracellular Persisters. Based on the metabolomics results, we next investigated the changes in ATP content in both planktonic and intracellular persisters following treatment with

https://doi.org/10.1021/acsnano.5c06864
ACS Nano XXXX, XXX, XXX−XXX

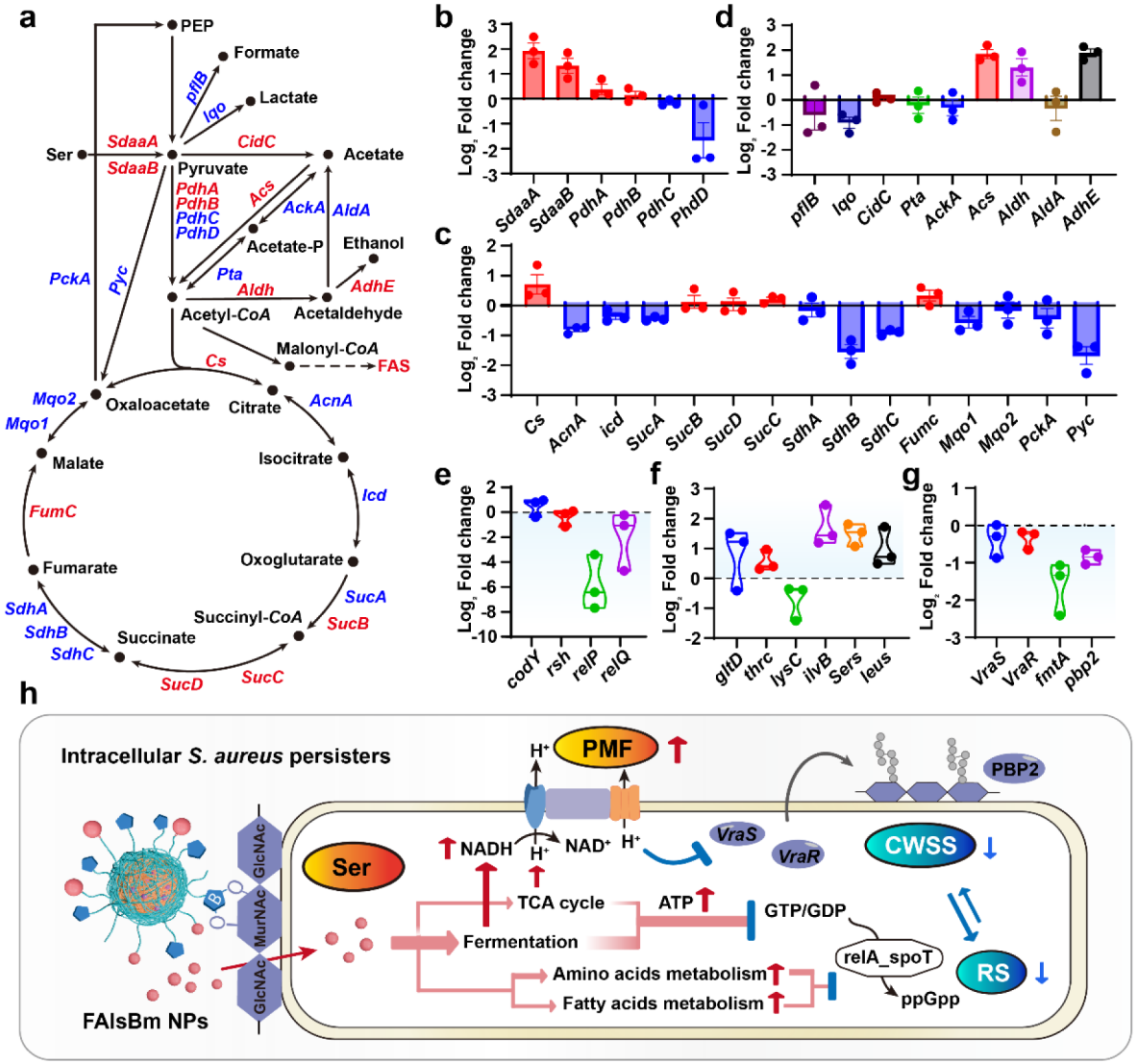

Figure 7. FAlsBm NPs reprogramed the metabolism of intracellular persisters. a) Schematic representation of genes involved central carbon metabolism. qPCR analysis of gene expression related to b) Ser metabolism, c) the TCA cycle, d) fermentation, e) SR, f) amino acid metabolism, and g) CWSS. h) Schematic overview of the pathways through which on-site delivered Ser triggers the switch in persistent phenotype of intracellular *S. aureus*. The cells used in the experiment were the murine-derived macrophage cell line Raw264.7. Data are means ± SEM (b–g) of three independent experiments. (b–g) Source data are provided as a Source Data file. Statistical significance was determined by unpaired *t* test (two-tailed). **** $p < 0.0001$, *** $p < 0.001$, ** $p < 0.01$, * $p < 0.05$, ns $p > 0.05$.

exogenous Ser, FAlB NPs, and FAlsBm NPs. In planktonic persisters, ATP levels showed a slight but nonsignificant decrease compared to those in susceptible bacterioplankton ($p = 0.0639$; Figure 6a). Upon treatment with exogenous Ser, an upregulation in ATP content was observed in the persisters. Significantly, the highest ATP levels were seen with FAlsBm NP treatment ($p = 0.0070$, **). A similar pattern was observed in intracellular persisters (Figure 6b), where ATP content production was significantly enhanced following FAlsBm NP treatment ($p = 0.0038$, **). These findings aligned with the metabolomics results, confirming that FAlsBm NPs modulated the metabolism of the *S. aureus* persister. This modulation likely occurred through the bacterial conversion of Ser delivered on-site by FAlsBm NPs, thereby inducing a metabolic shift in intracellular *S. aureus* persisters. Notably, metabolomics analysis suggested that delivered Man might also contribute to ATP content through glycolysis pathways. Interestingly, the FAlB NPs also increased ATP content in persisters, possibly due to cell wall perturbation caused by their targeted interaction with bacterial peptidoglycan, which altered PMF and metabolism by alleviating cell wall stress.[37]

Moreover, FAlsBm NPs contributed to the generation of NADH within the intracellular persisters (Figure 6c,d). The NADH/NAD^+ ratio after treatment with FAlsBm NPs (2.80) was 2.07-fold and 3.97-fold higher than those treated with exogenous Ser (1.35, $p = 0.0844$) and FAlB NPs (0.71, $p = 0.0289$, *), respectively. NADH is readily oxidized by enzymes in the electron transport chain, which in turn promotes the production of PMF.[15,38] The survival of *S. aureus* in host cells, indeed of all pathogens in any environment, requires the generation of both ATP and PMF across the cytoplasmic membrane.[39,40] To assess the PMF, the dye $DiOC_2(3)$ was used to measure the bacterial membrane potential. $DiOC_2(3)$ emits green fluorescence but shifts to red fluorescence as it accumulates and self-polymerizes within the bacterial membrane.[15] When the bacterial membrane potential is high, the

https://doi.org/10.1021/acsnano.5c06864
ACS Nano XXXX, XXX, XXX−XXX

red fluorescence intensity increases. As shown in Figure 6e, intracellular *S. aureus* persisters displayed bright yellow fluorescence due to the merging of green and red signals emitted by $DiOC_2(3)$. Similarly, no notable change in fluorescence was observed in intracellular persisters treated with Ser, indicating that the cellular uptake of Ser was restricted by the host cell metabolic feedback. FAlB NPs slightly enhanced the red/green fluorescence intensity ratio, suggesting a mild perturbation of the cell membrane by FAlB NPs. Conversely, FAlsBm NPs notably increased the red/green fluorescence intensity ratio, with intracellular persisters showing bright red fluorescence, which strongly demonstrated that on-site delivery of Ser by FAlsBm NPs overcame metabolic feedback inhibition in host cells, effectively increasing the PMF of intracellular *S. aureus* persisters. To further elucidate PMF fluctuation, planktonic persisters were sequentially treated with the proton ionophore carbonyl cyanide *m*-chlorophenyl hydrazine (CCCP),[15] which dissipates membrane potential by removing the proton gradient, and then incubated with FAlsBm NPs (Figure 6f). Since persistent bacteria are metabolically inactive, CCCP treatment had a minimal impact on their fluorescence intensity. In contrast, FAlsBm NP treatment significantly diminished the green fluorescence intensity of persisters (p = 0.0028, **), highlighting PMF reinforcement by FAlsBm NPs. Furthermore, increasing CCCP concentration led to a dose-dependent increase in green fluorescence, indicating that the PMF induced by FAlsBm NPs was inhibited by CCCP (Figure 6f). Notably, fluorescence changes were significantly more pronounced in the FAlsBm NP (or FAlsBm@Rif NP)-treated group compared with the Ser or Ser plus Rif groups, where changes were negligible (Figure 6f,6g). These findings demonstrate that FAlsBm NPs effectively activated intracellular persisters by boosting ATP production, generating NADH, and strengthening PMF, which collectively promoted Rif killing against persisters.

FAlsBm NPs Alleviate SR and CWSS in Intracellular Persisters by Strengthening the Fermentation Pathway. Previous studies have shown that exogenous amino acids enhance TCA cycle activity in planktonic persisters, leading to increased ATP production.[26] To invert the impact of FAlsBm NPs on the intracellular persister, we analyzed the expression of enzymes associated with central carbon metabolic pathways (Figure 7a). Quantitative PCR (qPCR) revealed significant upregulation of the expression of *SdaaA* and *SdaaB* (Figure 7b), which converted Ser delivered by FAlsBm NPs into pyruvate through dehydration and deamination. The pyruvate dehydrogenase complex then catalyzed the oxidative decarboxylation of pyruvate to produce acetyl-CoA, a key intermediate in initiating the TCA cycle. Interestingly, most TCA cycle-related genes did not exhibit significant expression changes, whereas genes associated with ATP and NADH production, such as *SucB*, *SucC*, and *SucD*, were markedly upregulated (Figure 7c). Conversely, genes involved in fermentation pathways showed significant upregulation following FAlsBm NP treatment. This observation highlighted the metabolic adaptability of intracellular *S. aureus* persisters in response to reactive oxygen species (ROS) and host immune defenses.[41,42] Under these conditions, respiration is reduced, and bacteria redirect their metabolism toward fermentation. Notably, FAlsBm NPs induced the expression of genes involved in fermentation, including *cidC* (pyruvate oxidase), *Aldh* (aldehyde dehydrogenase), and *AdhE* (alcohol dehydrogenase), in intracellular persisters (Figure 7d). These enzymes facilitated the conversion of pyruvate and acetyl-CoA into acetate and ethanol, suggesting that intracellular persisters increasingly relied on fermentation for energy production.

Beyond energy production, the Ser provided by FAlsBm NPs contributed to reversing the persistent phenotype. The accumulation of acetyl-CoA enhanced lipid catabolism and promoted the synthesis of fatty acids (Figures 7a and 5e). Fatty acids can repress the expression of SaeRSPQ, a regulator of virulence factors such as a-toxin, which is linked to the persistent phenotype.[39] Consistent with this, the activation of the SR, which is commonly associated with persistence, was significantly inhibited,[43,44] as evidenced by the reduced expression of related genes such as the *CodY* regulon and enzymes like *Rsh*, *RelP*, and *RelQ*, involved in the synthesis of alarmones (p)ppGpp (Figure 7e). Furthermore, genes associated with amino acid metabolism,[45] such as *gltD* (glutamate synthase, small subunit), *thrC* (threonine synthase), *lysC* (aspartokinase II), *ilvB* (acetolactate synthase large subunit), *Sers* (seryl-tRNA synthetase), and *LeuS* (leucyl-tRNA synthetase), were generally repressed in response to the SR stimulon. However, these genes were significantly upregulated in the presence of FAlsBm NPs (Figure 7f), further indicating the alleviation of RS.

Additionally, intracellular persisters undergo extensive reprogramming of peptidoglycan biosynthesis-related gene expression, initiating a protective response to cell wall defects known as bacterial CWSS. This response involves markedly elevated expression of genes such as *fmtA* (a penicillin-binding protein with a low affinity for β-lactams) and *pbp2* (involved in transglycosylation). Moreover, the *vraS*/*vraR* two-component system serves as a critical marker for CWSS, where *VraS* activates the response regulator *VraR* by phosphorylation in response to stress signals.[46] However, upon treatment with FAlsBm, bacterial CWSS was alleviated, as indicated by the reduced expression of *VraS*, *VraR*, *fmtA*, and *pbp2* (Figure 7g).

Our findings demonstrate that on-site delivery is a promising strategy for combating intracellular *S. aureus* persisters. Unlike planktonic persistent bacteria, intracellular persisters reside within host cells, forming substantial barriers that impede drug and nutrient uptake. The acidic intracellular environment compromises drug activity, while host cell metabolic restrictions limit the availability of nutrient supplementation for bacterial metabolism.[19,29] Although the combination of Ser and Rif does not significantly enhance the eradication of intracellularly persistent *S.aureus*, we identify a more effective approach using FAlsBm@Rif NPs. FAlsBm@Rif NPs specifically target macrophages via Man-mediated endocytosis. Upon cellular uptake, the acidic environment within the phagolysosome triggers the detachment of Man, exposing phenylboronic acid groups. These groups facilitate lysosomal escape and direct the NPs to intracellular bacteria through peptidoglycan-specific binding. This on-site delivery enables precise release of Ser and Rif at the site of intracellular persisters, overcoming barriers posed by host cell membranes and nutrient deprivation, and promoting targeted action against intracellular persisters. Furthermore, FAlB NPs serve as a versatile platform capable of carrying any type of amino acids and sugars through robust Schiff base bonds and boronic acid ester linkages, providing a valuable tool for investigating the effects and mechanism of drug combinations against intracellular persistent bacteria.

https://doi.org/10.1021/acsnano.5c06864
ACS Nano XXXX, XXX, XXX−XXX

We present evidence of metabolic reprogramming in intracellular *S. aureus* persisters facilitated by the on-site delivered Ser. Specifically, Ser activates the fermentation pathway in these persisters, driving a metabolic shift that enhances ATP production and the PMF, ultimately reversing persistence, as evidenced by reduced SR and CWSS (Figure 7h). Our findings confirm that intracellular *S. aureus* persisters predominantly rely on fermentation rather than the TCA cycle, likely due to the downregulation of aerobic respiration in response to phagocyte oxidative stress and host defense mechanisms. A previous study has suggested that the formation of intracellular persistence is not driven by a lack of ATP or amino acids.[12] Rather, intracellular *S. aureus* adopts a persistent phenotype to adapt to host defenses and evade antibiotic treatment. Under oxidative stress, the delivered Ser plays a crucial role in fostering redox balance, as supported by the increased intracellular bacterial NADH/NAD^+ ratio and enhanced PMF observed in an in situ model of persistent bacteria. Therefore, while sensitizing intracellular persisters to antibiotic killing by enhancing bacterial metabolism is promising, this approach is constrained by the efficiency of the fermentation pathway. This pathway relies on the modulation of redox homeostasis and the electron transport chain, which in turn influences the reversal of persistence. Consequently, approaches aimed at reversing oxidative stress or directly modulating bacterial electron transport via on-site delivery might augment the efficacy of antibiotic treatment or potentially eradicate intracellular persisters without antibiotics.

CONCLUSIONS

In summary, we proposed an on-site delivery strategy to enhance the antibiotic susceptibility of intracellular *S. aureus* persisters through amino acid-induced metabolic activation. FAlsBm NPs demonstrated dual-targeting capabilities for host cells and intracellular *S. aureus* persisters, effectively overcoming host cell membrane barriers and achieving precise codelivery of Ser and Rif directly to the intracellular persister loci. The delivered Ser bypassed host cellular metabolic constraints, inducing a metabolic shift in intracellular *S. aureus* persisters. This shift transitioned the bacteria from a dormant to an active state by stimulating fermentation pathways, increasing ATP production, and reinforcing membrane potential. This metabolic reprogramming effectively mitigated both SR and CWSS, two key mechanisms underlying bacterial persistence. As a result, FAlsBm@Rif NPs achieved superior elimination of intracellular persisters in both in vitro and in vivo studies, significantly outperforming all control groups, including free Rif, free MOX, Rif+Ser, and FAlB@Rif NPs. This study not only introduces an on-site delivery strategy tailored for intracellularly persistent bacteria but also provides an in-depth mechanistic understanding of the reversal of persistence, offering new insights and approaches for combating intracellular bacterial persisters.

MATERIALS AND METHODS

Material. D-Phenylalanine (≥98%), *p*-aldehyde benzoic acid (≥98%), Ser (≥98%), Ala (≥98%), Man (≥98%), 2-hydroxyethyl acrylate (≥98%), 2-[dodecylthiothio-(thiocarbonyl)thio]-2-methylpropionic acid (DDMAT, ≥98%), tris(2-phenylpyridine)iridium (Ir(ppy)3, ≥98%), Rif (≥98%), *N*,*N*'-dicyclohexylcarbodiimide (DCC, ≥98%), 4-dimethylaminopyridine (DMAP, ≥98%), and 2-hydroxyethyl acrylate (HEA, ≥ 98%) were purchased from the Tokyo Chemical Industry Union (TCI), while 4-boron-L-phenylalanine (≥98%), gentamicin (Gen, ≥ 98%), Mox (≥98%), and Van (≥98%) were purchased from Mereda (China). Commonly used solvents such as DMSO, ethanol (EtOH), tetrahydrofuran (THF), *n*-hexane (HEX), trifluoroacetic acid (TFA), ethyl acetate (EA), and sodium dodecyl sulfate (SDS) were purchased from J&K Scientific. Trypsin Soy Broth (TSB), Trypsin Soy Agar (TSA), M9 medium, Mueller−Hinton Broth (MHB), Hanks' buffered saline solution (HBSS), bovine serum albumin (BSA), lysostaphin, and Triton X-100 were purchased from Sinopharm Chemical Reagents (China).

Cell culture media were purchased from Gibco BRL (United States) and CORNING (U.S.A.). Thiazolyl Blue Tetrazolium Bromide (MTT), Lyso-Tracker Red, DAPI, FITC, and 3−3 diethyloxacarbacyanidanthocyanide iodine ($DiOC_2(3)$) were obtained from Solar Science & Technology Co. Ltd. (China).

A *Staphylococcus aureus* RNA Rapid Extraction Kit (spin column) was purchased from Beijing Junod Biotechnology Co., Ltd.; the NovoScript Plus All-in-one first Strand cDNA Synthesis SuperMix (gDNA Purge) Kit and NovoStart SYBR qPCR SuperMix Plus Kit were purchased from Nearshore Protein (China). The ATP content kit and Coenzyme I NAD(H) Assay Kit were purchased from Solaibao (China).

Bacterial Culture. MRSA 1857 used in this study, isolated from the Affiliated Hospital of the Chinese Academy of Military Medical Sciences,[29] was incubated in the TSB medium for 9 h at 37 °C with shaking at 180 rpm. The suspension was then centrifuged at 7,500 rpm for 3 min, washed twice with saline, and resuspended in saline for storage at 4 °C.

Planktonic Bacteria Killing Curves. To evaluate planktonic bacteria killing curves, 100 μL of MRSA in exponential growth was added to 100 mL of fresh MHB. For sensitive bacteria, 50× MIC Van was added; for resistant bacteria, 10 × MIC Amo was used. For persistent bacteria, 100 μL of planktonic persisters and 50× MIC Van were inoculated into 100 mL of M9 medium. All cultures were incubated at 37 °C with shaking at 180 rpm. Samples were collected at 0, 2, 4, 6, 8, and 12 h, washed three times with saline, and diluted for drop plate counting on TSA plates.

Extracellular Antibacterial Evaluation. A 100 μL aliquot of the bacterial suspension was added to 100 mL of MHB and incubated at 37 °C while being shaken at 180 rpm for 12 h. A portion of this culture solution, specifically, 40 mL, was treated with 50× MIC Van and subsequently incubated under the same conditions for an additional 8 h. The bacteria were then centrifuged, washed twice with M9 medium, and resuspended in M9 medium to obtain planktonic persisters. These persisters were coincubated with varying concentrations of drugs, amino acids (Ser and Ala), or FAlsBm@Rif NPs in M9 medium at 37 °C for 24 h. After incubation, the cultures were washed twice with M9 medium, diluted stepwise, and plated on TSA plates for drop plate counting.

MIC Test. TSB medium (100 μL) with 2-fold serial dilutions of various drugs was added to a 96-well plate. MRSA or planktonic bacteria were diluted to 5×10^6 CFU/mL, and 100 μL of this suspension was added to each well. After incubating at 37 °C for 24 h, the OD600 of the cultures was measured using a plate reader. TSB containing only bacteria served as a positive control, while TSB without bacteria was used as a negative control.

Cell Culture. The murine-derived macrophage cell line Raw264.7 was selected for the experiments, and Raw264.7 was

https://doi.org/10.1021/acsnano.5c06864
ACS Nano XXXX, XXX, XXX−XXX

cultured in high-sugar DMEM containing 10% fetal bovine serum (FBS) and 1% penicillin−streptomycin (P/S) solution under a humidified atmosphere of 5% CO_2 at 37 °C.

Cytotoxicity Assay. Raw264.7 macrophages were seeded in 96-well plates at a density of 1×10^4 cells/well. After overnight incubation, the cells were treated with different concentrations of FAlB NPs (or FAlsBm NPs) for 24 and 48 h. Following treatment, 10 μL of MTT (5 mg/mL) was added to each well, and the mixture was incubated for 4 h. Subsequently, 100 μL of 10% SDS was added to each well, and the mixture was incubated for 12 h. Absorbance was measured at 570 nm.

Intracellular Persister Bacteria Model. Raw264.7 macrophages were seeded in 24-well plates at a density of 1×10^5 cells/well and cultured overnight. After being washed three times with PBS, the medium was replaced with MRSA-containing RPMI 1640 with 10% FBS, allowing for a 1 h incubation at a multiplicity of infection (MOI) of 10:1. The MRSA-containing medium was then removed, and the cells were washed three times with PBS. To eliminate extracellular bacteria, RPMI 1640 with 10% FBS containing Gen (50 μg/mL) was added for 1 h. Afterward, the cells were rinsed three times with PBS and replaced with fresh RPMI 1640 containing 10% FBS to obtain intracellular bacteria. For the intracellular persistent bacteria, Van at 50× MIC was added, and the cells were incubated for 24 h, followed by three washes with PBS. The resulting cells were termed intracellular persisters.

Intracellular Persisters Killing Curves. After intracellular persisters were obtained, the RPMI 1640 medium with 10% FBS containing 10× MIC Rif was added. At 0, 2, 4, 6, 8, and 12 h, the medium was aspirated, and the cells were washed three times with PBS. The cells were then lysed by adding 0.1% Triton X-100 for 10 min, and the bacteria were collected and quantified by drop plating on TSA plates.

Intracellular Antibacterial Evaluation. After intracellular persisters, amino acids (Ser and Ala) or FAlsBm NPs, or FAlB NPs, were coincubated for 24 and 48 h. The medium was then aspirated, and the cells were washed three times with PBS. Cells were lysed by adding 0.1% Triton X-100 for 10 min, and the bacteria were collected and quantified by drop plating on TSA plates.

Synthesis of the Monomers. *α*-*N*-acryloyl-D-phenylalanine monomer (denoted as F) and (*S*)-2-acrylamido-3-(4-boronophenyl)propionic acid monomer (denoted as B) were synthesized according to a previously reported method. The synthesis of ethyl 2-((4-formylbenzyl)oxy)acrylate (denoted as Al) monomers was carried out as follows: briefly, 2.0 g (13.3 mM) of p-formylbenzoic acid, 2.3 g (19.8 mM) of 2-hydroxyethyl acrylate, 4.9 g (25.6 mM) of DCC, and 0.3 g (2.5 mM) of DMAP were weighed and added to 20 mL of ultradry THF. After 24 h at room temperature, the reaction mixture was extracted, filtered, and then rotary evaporated. The colorless oily product was separated by column chromatography in a mobile phase of hexane:ethyl acetate in 3:1. The monomers were all successfully synthesized and characterized by ^{1}H NMR and ESI-MS.

Synthesis of FAlB. Poly(*N*-acryloyl phenylalanine) (denoted as PF) was synthesized as previously reported. Then, PF was used as macro-CTA for the synthesis of poly(acryloyl-D-phenylalanine)-*block*-poly(2-((4-formylbenzyl)oxy)ethyl acrylate) (denoted as PFAl) with the usual monomers Al (0.2 g, 0.81 mM), PF (0.12 g, 0.0162 mM), and Ir(ppy)$_3$ (0.0052 mg, 8×10^{-6} mM) were dissolved in 1 mL of ultradry DMSO. The reaction was blown N_2 for 30 min and then reacted under blue light for 6 h. PFAl was obtained after being dried by dialysis. Poly(*N*-acryloyl phenylalanine)-*b*-poly(2-((4-formylbenzyl)oxy) acrylic acid ethyl ester)-*b*-poly((S)-2-acrylamido-3-(4-boronphenyl) propionic acid) (denoted as FAlB) was also synthesized by the polymerization method of PET-RAFT with PFAl as macro-CTA, usually by dissolving monomer B (0.1 g, 0.38 mM), PFAl (0.1 g, 0.0076 mM), and Ir(ppy)$_3$ (0.005 mg, 7.6×10^{-6} mM) in 700 μL of ultradry DMSO, followed by blowing N_2 for 30 min and reacting under blue light for 10 h. FAlB was obtained after drying by dialysis.

Synthesis of FAlsBm. 10 mg of polymer FAlB was dissolved in 1 mL of ultradry DMSO, and 5 mg of Ser and 1 μL of TFA were added and stirred at 37 °C. After the reaction overnight, 5 mg of Man was added, and after 8 h of reaction, the product was dialyzed and obtained as FAlsBm.

Preparation of NPs. Take 10 mg of FAlB (or FAlsBm) and 1 mg of Rif, mix and dissolve them in 1 mL of DMSO. To this solution, 10 mL of deionized water was slowly added dropwise with high-speed stirring while dropping. After high-speed stirring for 30 min, the NPs were collected from the dialysis bag (MWCO: 3500 Da) after 48 h of sterile water dialysis and were named FAlB@Rif NPs (or FAlsBm@Rif NPs). FAlB@NR NPs, FAlsBm@NR NPs, FAlB@FITC NPs, and FAlsBm@FITC NPs were also prepared according to this method. The size, potential, morphology, and stability of the nanoparticles were evaluated by DLS/TEM.

Rif Release Curve. FAlsBm@Rif NPs were dispersed in 1 mL of PBS solution (5 mg/mL) at pH values of 4.5, 5.5, 6.5, and 7.2. The dispersions were placed in dialysis bags (MWCO: 3500 Da) and immersed in 5 mL of PBS buffer at the corresponding pH. This dialysis system was incubated in a shaker at 37 °C. At specified time intervals, 1 mL of the external solution was collected, and an equal volume of PBS buffer at the corresponding pH was added. UV−vis analysis was conducted at 483 nm.

Time-Dependent Cellular Internalization. Macrophages Raw264.7 were inoculated into confocal culture dishes at a density of ∼10^5 cells/well. After overnight incubation, FAlsBm@NR NPs (NR 5 μg/mL) were added to the medium at different times to coincubate with the cells. The cells were washed with PBS after the incubation was completed, and finally, the cells were fixed with 4% paraformaldehyde (20 min), stained with DAPI (10 min), and then observed by CLSM. The MFI of the cells was analyzed by ImageJ software.

Competitive Uptake Inhibition Mediated by Man. Raw264.7 macrophages were seeded in confocal culture dishes at a density of ∼10^5 cells/well and incubated overnight. Different concentrations of Man (1 and 2 mg/mL) and fresh RPMI 1640 medium with 10% FBS were then added, and the cells were incubated for 2 h. Following this, the cells were washed three times with PBS, and fresh RPMI 1640 medium with 10% FBS containing FAlsBm@NR NPs (NR 5 μg/mL) was added for 3 h coincubation. After washing with PBS, the cells were fixed with 4% paraformaldehyde for 20 min, stained with DAPI for 10 min, and observed using CLSM. The MFI of the cells was analyzed using ImageJ software.

Lysosomal Escape. Raw264.7 macrophages were seeded in confocal culture dishes at a density of 2×10^5 cells/plate and incubated overnight. FAlsBm@FITC NPs were then added, and the cells were coincubated for 24 h, followed by three washes with PBS. Subsequently, LysoTracker was added and incubated for 1 h. The cells were washed with PBS, fixed

https://doi.org/10.1021/acsnano.5c06864
ACS Nano XXXX, XXX, XXX−XXX

with 4% paraformaldehyde, stained with DAPI, and imaged using CLSM at various time points. The Pearson correlation coefficient (PCC), overlap coefficient (OVL), and regional coexistence fluorescence spectra were analyzed by using ImageJ software.

Intracellular Bacterial Targeting. Cells were infiltrated with FITC-MRSA to construct the intracellular bacteria. Following intracellular bacterial development, the RPMI 1640 medium with 10% FBS containing FAlsBm@NR (NR 5 μg/mL) was added. After 24 h, the medium was removed, and the cells were washed three times with PBS. The cells were then fixed with 4% paraformaldehyde and stained with DAPI before being observed using CLAM. The regional coexistence fluorescence spectrum was analyzed using ImageJ software.

Mouse Treatment. Balb/c female mice (8 weeks old) were purchased from Beijing Charles River Co., Ltd. All animals were treated and cared for under the National Research Council's Guide for the Care and Use of Laboratory Animals and under proper supervision.

Biosafety Analysis. Mice were randomly divided into five groups (n = 3 per group) and treated via tail vein injection with PBS, Rif, Van, Rif + Ser, and FAlsBm@Rif NPs (Rif 10 mg/kg) every 2 days. The mice were weighed throughout the experiment, and on day 10, they were euthanized for biochemical analysis. Major organs, including the liver, spleen, lungs, and kidneys, were collected and assessed using hematoxylin and eosin (H&E) staining.

In Vivo Antibacterial Efficacy (*S. aureus* Persister-Induced Peritonitis Model). Mice were injected intraperitoneally with a bacterial solution (10^8 CFU in 100 μL of PBS) and incubated for 6 h. Following this, 75 mg/kg Van was administered intraperitoneally to induce persistent bacteria. After an additional 18 h incubation, mice were treated with different drug groups including PBS, Rif, Rif + Ser, and FAlsBm@Rif NPs (10 mg/kg Rif) via intraperitoneal injection. After 24 h, 2 mL of HBSS was administered intraperitoneally, and the mice were euthanized. The peritoneal fluid was collected to determine total, extracellular, and intracellular CFUs. One-third of the peritoneal fluid was used to quantify total CFUs. Another third was centrifuged, and the supernatant was collected to quantify extracellular CFUs. The final third was incubated with lysozyme (15 μg/mL) to kill extracellular MRSA, followed by lysis with HBSS containing 0.1% Triton X-100 to quantify intracellular CFUs. Additionally, major organs, including the heart, liver, spleen, lungs, and kidneys, were evaluated using H&E staining.

Metabolomics Analysis of Intracellular Persisters Treated with or without FAlsBm NPs. RAW264.7 macrophages were seeded in culture plates at a density of 10^8 cells/plate and then infiltrated and induced to obtain intracellularly persistent cells. A fresh RPMI 1640 medium with 10% FBS and Van containing FAlsBm NPs (19.8 μg/plate) were added separately and coincubated for 12 h. After incubation, the medium was removed, and the cells were washed three times with PBS. The cells were then lysed with 0.1% Triton X-100, and the intracellular bacteria were collected. Following centrifugation at 7,500 rpm for 5 min, the bacterial pellet was washed twice with precooled PBS. The supernatant was discarded, and the bacteria were resuspended in 1.5 mL centrifuge tubes, snap-frozen in liquid nitrogen for 15 min, and stored at −80 °C for transport on dry ice. The samples were entrusted to Novozymes for testing.

ATP Measurement. Planktonic persisters were coincubated with Ser, FAlB, and FAlsBm in M9 medium at 37 °C for 24 h. Bacteria were then collected into 1.5 mL centrifuge tubes and analyzed for ATP content using a Solebel ATP assay kit.

RAW264.7 macrophages were seeded in culture plates at a density of 10^8 cells/plate, and then infiltrated and induced to obtain intracellularly persistent cells. Following this, fresh RPMI 1640 medium with 10% FBS containing Van, Ser, FAlB NPs, and FAlsBm NPs was added, and the cells were coincubated for 12 h. The medium was removed, and the cells were washed three times with PBS. The cells were lysed with 0.1% Triton X-100, and intracellular bacteria were collected. The bacterial pellet was obtained by centrifugation at 7,500 rpm for 5 min, and ATP content was measured using the Solebel ATP assay kit.

PMF Determination. Planktonic persisters were coincubated with varying concentrations of CCCP, along with Van, Ser, FAlB NPs, FAlsBm NPs, Rif, Rif + Ser, FAlB@Rif NPs, and FAlsBm@Rif NPs for 24 h. $DiOC_2(3)$ dye was then added and incubated for 15 min at 37 °C. Fluorescence was analyzed using a fluorescence enzyme marker with excitation/emission wavelengths of 482/497 nm.

After obtaining the intracellular persisters, fresh RPMI 1640 medium with 10% FBS containing Van, Ser, FAlB NPs, and FAlsBm NPs was added separately and coincubated for 12 h. The medium was removed, and the cells were washed three times with PBS. Following fixation with 4% paraformaldehyde and staining with $DiOC_2(3)$, fluorescence spectra were observed using CLAM, and regional coexistence was analyzed using ImageJ software.

Intracellular Persisters NAD^+ and NADH Assay. RAW264.7 macrophages were seeded in culture plates at a density of 10^8 cells/plate, and then infiltrated and induced to obtain intracellularly persistent cells. RPMI 1640 medium with 10% FBS containing Van, Ser, FAlB NPs, and FAlsBm NPs was then added, and the cells were coincubated for 12 h. After incubation, the medium was removed, and the cells were washed three times with PBS. The cells were lysed with 0.1% Triton X-100, and intracellular bacteria were collected. The bacterial pellet was obtained by centrifugation at 7,500 rpm for 5 min, and NAD^+ and NADH content was measured using the Coenzyme I NAD(H) Assay Kit from Solebel.

qPCR Assay. After obtaining intracellular persisters, the organisms were collected separately in 1.5 mL centrifuge tubes; bacterial RNA was extracted, and the extracted RNA was converted to cDNA for the qPCR. The 2(-ΔΔCt) method with gmk as the housekeeping gene was used to determine the fold change of the expressed gene from the control condition.

Statistical Methods. Colocalization analysis and gap area calculation were performed by using the ImageJ software. Data are shown as mean ± SEM of independent biological replicates. Statistical analyses were performed using GraphPad Prism, employing the statistical methods indicated in the figure legends. In this work, Figure 6f,g was used to compare the differences between the means of the groups using the paired t test (two-tailed), and the other data were compared using the unpaired t test (two-tailed). **** $p < 0.0001$, *** $p < 0.001$, ** $p < 0.01$, * $p < 0.05$, ns $p > 0.05$.

ASSOCIATED CONTENT

Supporting Information

The Supporting Information is available free of charge at https://pubs.acs.org/doi/10.1021/acsnano.5c06864.

https://doi.org/10.1021/acsnano.5c06864
ACS Nano XXXX, XXX, XXX−XXX

Construction and evaluation of planktonic and intracellular persisters; synthesis and characterization of polymers and NPs; interaction of FAlsBm NPs with cells; evaluation of in vivo animal safety of FAlsBm@Rif NPs (PDF)

AUTHOR INFORMATION

Corresponding Authors

Guofeng Li − *State Key Laboratory of Organic−Inorganic Composites, Beijing Laboratory of Biomedical Materials, Beijing University of Chemical Technology, Beijing 100029, PR China;* orcid.org/0000-0002-4101-0059; Email: ligf@mail.buct.edu.cn

Xing Wang − *State Key Laboratory of Organic−Inorganic Composites, Beijing Laboratory of Biomedical Materials, Beijing University of Chemical Technology, Beijing 100029, PR China;* orcid.org/0000-0002-9990-1479; Email: wangxing@mail.buct.edu.cn

Authors

Diandian Huang − *State Key Laboratory of Organic−Inorganic Composites, Beijing Laboratory of Biomedical Materials, Beijing University of Chemical Technology, Beijing 100029, PR China*

Xiaoxu Kang − *State Key Laboratory of Organic−Inorganic Composites, Beijing Laboratory of Biomedical Materials, Beijing University of Chemical Technology, Beijing 100029, PR China; Institute of Clinical Medicine, China-Japan Friendship Hospital, Beijing 100029, PR China*

Zibo Yin − *State Key Laboratory of Organic−Inorganic Composites, Beijing Laboratory of Biomedical Materials, Beijing University of Chemical Technology, Beijing 100029, PR China*

Dongdong Zhao − *State Key Laboratory of Organic−Inorganic Composites, Beijing Laboratory of Biomedical Materials, Beijing University of Chemical Technology, Beijing 100029, PR China*

Yuchen Ning − *State Key Laboratory of Organic−Inorganic Composites, Beijing Laboratory of Biomedical Materials, Beijing University of Chemical Technology, Beijing 100029, PR China*

Huan Liu − *State Key Laboratory of Organic−Inorganic Composites, Beijing Laboratory of Biomedical Materials, Beijing University of Chemical Technology, Beijing 100029, PR China*

Feng Li − *Department of Orthopaedics, Peking University Third Hospital, Beijing 100082, PR China*

Wensheng Xie − *State Key Laboratory of Organic−Inorganic Composites, Beijing Laboratory of Biomedical Materials, Beijing University of Chemical Technology, Beijing 100029, PR China*

Complete contact information is available at: https://pubs.acs.org/10.1021/acsnano.5c06864

Author Contributions

#D.H. and X.K. contributed equally to this work. G.L. and X.W. conceived the project. G.L., X.W., D.H., and X.K. designed the experiments. D.H. and X.K. performed the experimental work and analyzed the data with the help of Z.Y. and D.Z., and qPCR assessments were performed with the help of Y.N. and H.L. In vivo assessments were performed with the help of F.L.

Notes

The authors declare no competing financial interest.

ACKNOWLEDGMENTS

This work was supported by the National Natural Science Foundation of China (22275013, 52273118), the Fundamental Research Funds for the Central Universities (PY2508), and the Joint Project of BRC-BC (Biomedical Translational Engineering Research Center of BUCT-CJFH) (XK2023-16). All animals were treated and cared for in accordance with the National Research Council's Guide for the Care and Use of Laboratory Animals and under the supervision and assessment by GemPharmatech Co., Ltd. (Approval No. GPT-BJAP20250110-4). The authors thank Junfeng Liu and Zhengjun Li from BUCT for their help with the metabolic pathway analysis.

REFERENCES

(1) Fu, J.; Li, Y.; Zhang, Y.; Liang, Y.; Zheng, Y.; Li, Z.; Zhu, S.; Li, C.; Cui, Z.; Wu, S. An Engineered Pseudo-Macrophage for Rapid Treatment of Bacteria-Infected Osteomyelitis via Microwave-Excited Anti-Infection and Immunoregulation. *Adv. Mater* **2021**, *33* (41), 2102926.

(2) Kang, X.; Bu, F.; Feng, W.; Liu, F.; Yang, X.; Li, H.; Yu, Y.; Li, G.; Xiao, H.; Wang, X. Dual-Cascade Responsive Nanoparticles Enhance Pancreatic Cancer Therapy by Eliminating Tumor-Resident Intracellular Bacteria. *Adv. Mater* **2022**, *34* (49), 2206765.

(3) Meng, L.; Yang, F.; Pang, Y.; Cao, Z.; Wu, F.; Yan, D.; Liu, J. Nanocapping-enabled charge reversal generates cell-enterable endosomal-escapable bacteriophages for intracellular pathogen inhibition. *Sci. Adv* **2022**, *8* (28), No. eabq2005.

(4) Kwon, H.-K.; Lee, I.; Yu, K. E.; Cahill, S. V.; Alder, K. D.; Lee, S.; Dussik, C. M.; Back, J.; Choi, J.; Song, L.; et al. Dual therapeutic targeting of intra-articular inflammation and intracellular bacteria enhances chondroprotection in septic arthritis. *Sci. Adv* **2021**, *7* (26), No. eabf2665.

(5) Trouillet-Assant, S.; Lelièvre, L.; Martins-Simões, P.; Gonzaga, L.; Tasse, J.; Valour, F.; Rasigade, J.-P.; Vandenesch, F.; Muniz Guedes, R. L.; Ribeiro de Vasconcelos, A. T.; Caillon, J.; Lustig, S.; Ferry, T.; Jacqueline, C.; Loss de Morais, G.; Laurent, F. Adaptive processes of Staphylococcus aureus isolates during the progression from acute to chronic bone and joint infections in patients. *Cell. Microbiol* **2016**, *18* (10), 1405−1414.

(6) Li, Y.; Liu, Y.; Ren, Y.; Su, L.; Li, A.; An, Y.; Rotello, V.; Zhang, Z.; Wang, Y.; Liu, Y.; et al. Coating of a Novel Antimicrobial Nanoparticle with a Macrophage Membrane for the Selective Entry into Infected Macrophages and Killing of Intracellular Staphylococci. *Adv. Funct. Mater* **2020**, *30* (48), 2004942.

(7) Xie, J.; Zhou, M.; Qian, Y.; Cong, Z.; Chen, S.; Zhang, W.; Jiang, W.; Dai, C.; Shao, N.; Ji, Z.; et al. Addressing MRSA infection and antibacterial resistance with peptoid polymers. *Nat. Commun* **2021**, *12* (1), 5898.

(8) Santucci, P.; Greenwood, D. J.; Fearns, A.; Chen, K.; Jiang, H.; Gutierrez, M. G. Intracellular localisation of Mycobacterium tuberculosis affects efficacy of the antibiotic pyrazinamide. *Nat. Commun* **2021**, *12* (1), 3816.

(9) Peyrusson, F.; Tulkens, P. M.; Bambeke, F. V. Cellular Pharmacokinetics and Intracellular Activity of Gepotidacin against Staphylococcus aureus Isolates with Different Resistance Phenotypes in Models of Cultured Phagocytic Cells. *Antimicrob. Agents Chemother* **2018**, *62* (4), 10−1128.

(10) Fanous, J.; Claudi, B.; Tripathi, V.; Li, J.; Goormaghtigh, F.; Bumann, D. Limited impact of *Salmonella* stress and persisters on antibiotic clearance. *Nature* **2025**, *639*, 181−189.

(11) Lewis, K. Persister cells, dormancy and infectious disease. *Nat. Rev. Microbiol* **2007**, *5* (1), 48−56.

(12) Peyrusson, F.; Varet, H.; Nguyen, T. K.; Legendre, R.; Sismeiro, O.; Coppée, J.-Y.; Wolz, C.; Tenson, T.; Van Bambeke, F. Intracellular Staphylococcus aureus persisters upon antibiotic exposure. *Nat. Commun* **2020**, *11* (1), 2200.
(13) Helaine, S.; Cheverton, A. M.; Watson, K. G.; Faure, L. M.; Matthews, S. A.; Holden, D. W. Internalization of *Salmonella* by Macrophages Induces Formation of Nonreplicating Persisters. *Science* **2014**, *343* (6167), 204−208.
(14) Blattman, S. B.; Jiang, W.; McGarrigle, E. R.; Liu, M.; Oikonomou, P.; Tavazoie, S. Identification and genetic dissection of convergent persister cell states. *Nature* **2024**, *636* (8042), 438−446.
(15) Allison, K. R.; Brynildsen, M. P.; Collins, J. J. Metabolite-enabled eradication of bacterial persisters by aminoglycosides. *Nature* **2011**, *473* (7346), 216−220.
(16) Peng, B.; Su, Y.-B.; Li, H.; Han, Y.; Guo, C.; Tian, Y.-M.; Peng, X.-X. Exogenous Alanine and/or Glucose plus Kanamycin Kills Antibiotic-Resistant Bacteria. *Cell Metab* **2015**, *21* (2), 249−262.
(17) Jiang, M.; Chen, X. H.; Li, H.; Peng, X. X.; Peng, B. Exogenous L-Alanine promotes phagocytosis of multidrug-resistant bacterial pathogens. *EMBO Rep* **2023**, *24* (12), No. e49561.
(18) Liu, Y.; Li, R.; Xiao, X.; Wang, Z. Bacterial metabolism-inspired molecules to modulate antibiotic efficacy. *J. Antimicrob. Chemother* **2019**, *74* (12), 3409−3417.
(19) Van den Bergh, B.; Schramke, H.; Michiels, J. E.; Kimkes, T. E. P.; Radzikowski, J. L.; Schimpf, J.; Vedelaar, S. R.; Burschel, S.; Dewachter, L.; Lončar, N.; et al. Mutations in respiratory complex I promote antibiotic persistence through alterations in intracellular acidity and protein synthesis. *Nat. Commun* **2022**, *13* (1), 546.
(20) Maghrebi, S.; Joyce, P.; Jambhrunkar, M.; Thomas, N.; Prestidge, C. A. Poly(lactic-co-glycolic) Acid−Lipid Hybrid Microparticles Enhance the Intracellular Uptake and Antibacterial Activity of Rifampicin. *ACS Appl. Mater. Interfaces* **2020**, *12* (7), 8030−8039.
(21) Huang, D.; Li, D.; Wang, T.; Shen, H.; Zhao, P.; Liu, B.; You, Y.; Ma, Y.; Yang, F.; Wu, D.; Wang, S. Isoniazid conjugated poly(lactide-co-glycolide): Long-term controlled drug release and tissue regeneration for bone tuberculosis therapy. *Biomaterials* **2015**, *52*, 417−425.
(22) Conlon, B. P.; Rowe, S. E.; Gandt, A. B.; Nuxoll, A. S.; Donegan, N. P.; Zalis, E. A.; Clair, G.; Adkins, J. N.; Cheung, A. L.; Lewis, K. Persister formation in Staphylococcus aureus is associated with ATP depletion. *Nat. Microbiol* **2016**, *1* (5), 16051.
(23) Allison, K. R.; Brynildsen, M. P.; Collins, J. J. Metabolite-enabled eradication of bacterial persisters by aminoglycosides. *Nature* **2011**, *473* (7346), 216−220.
(24) Fisher, R. A.; Gollan, B.; Helaine, S. Persistent bacterial infections and persister cells. *Nat. Rev. Microbiol* **2017**, *15* (8), 453−464.
(25) Niu, H.; Gu, J.; Zhang, Y. Bacterial persisters: molecular mechanisms and therapeutic development. *Signal Transduction Targeted Ther* **2024**, *9* (1), 174.
(26) Zhen, J.; Yan, S.; Li, Y.; Ruan, C.; Li, Y.; Li, X.; Zhao, X.; Lv, X.; Ge, Y.; Moure, U. A. E.; Xie, J. l-Alanine specifically potentiates fluoroquinolone efficacy against Mycobacterium persisters via increased intracellular reactive oxygen species. *Appl. Microbiol. Biotechnol* **2020**, *104* (5), 2137−2147.
(27) Duan, X.; Huang, X.; Wang, X.; Yan, S.; Guo, S.; Abdalla, A. E.; Huang, C.; Xie, J. l-Serine potentiates fluoroquinolone activity against *Escherichia coli*by enhancing endogenous reactive oxygen species production. *J. Antimicrob. Chemother* **2016**, *71* (8), 2192−2199.
(28) Eisenreich, W.; Heesemann, J.; Rudel, T.; Goebel, W. Metabolic host responses to infection by intracellular bacterial pathogens. *Front. Cell. Infect. Microbiol* **2013**, *3*, 24.
(29) Feng, W.; Li, G.; Kang, X.; Wang, R.; Liu, F.; Zhao, D.; Li, H.; Bu, F.; Yu, Y.; Moriarty, T. F.; et al. Cascade-Targeting Poly(amino acid) Nanoparticles Eliminate Intracellular Bacteria via On-Site Antibiotic Delivery. *Adv. Mater* **2022**, *34* (12), 2109789.
(30) Li, S.; Li, J.-J.; Zhao, Y.-Y.; Chen, M.-M.; Su, S.-S.; Yao, S.-Y.; Wang, Z.-H.; Hu, X.-Y.; Geng, W.-C.; Wang, W.; Wang, K.-R.; Guo, D.-S. Supramolecular Integration of Multifunctional Nanomaterial by Mannose-Decorated Azocalixarene with Ginsenoside Rb1 for Synergistic Therapy of Rheumatoid Arthritis. *ACS Nano* **2023**, *17* (24), 25468−25482.
(31) Gao, S.; Zhang, Y.; Zhou, R.; Shen, T.; Zhang, D.; Guo, Z.; Zou, X. Boronic acid-assisted detection of bacterial pathogens: Applications and perspectives. *Coord. Chem. Rev* **2024**, *518*, 216082.
(32) Ding, Y.; Hu, X.; Piao, Y.; Huang, R.; Xie, L.; Yan, X.; Sun, H.; Li, Y.; Shi, L.; Liu, Y. Lipid Prodrug Nanoassemblies via Dynamic Covalent Boronates. *ACS Nano* **2023**, *17* (7), 6601−6614.
(33) Zhang, W.; Wu, Y.; Liu, L.; Xiao, X.; Cong, Z.; Shao, N.; Qiao, Z.; Chen, K.; Liu, S.; Zhang, H.; Ji, Z.; Shao, X.; Dai, Y.; He, H.; Xia, J.; Fei, J.; Liu, R. The membrane-targeting mechanism of host defense peptides inspiring the design of polypeptide-conjugated gold nanoparticles exhibiting effective antibacterial activity against methicillin-resistant Staphylococcus aureus. *J. Mater. Chem. B* **2021**, *9* (25), 5092−5101.
(34) Lehar, S. M.; Pillow, T.; Xu, M.; Staben, L.; Kajihara, K. K.; Vandlen, R.; DePalatis, L.; Raab, H.; Hazenbos, W. L.; Hiroshi Morisaki, J.; Kim, J.; Park, S.; Darwish, M.; Lee, B.-C.; Hernandez, H.; Loyet, K. M.; Lupardus, P.; Fong, R.; Yan, D.; Chalouni, C.; et al. Novel antibody−antibiotic conjugate eliminates intracellular S. aureus. *Nature* **2015**, *527* (7578), 323−328.
(35) Yang, X.; Tang, X.; Yi, S.; Guo, T.; Liao, Y.; Wang, Y.; Zhang, X. Maltodextrin-derived nanoparticles resensitize intracellular dormant Staphylococcus aureus to rifampicin. *Carbohydr. Polym* **2025**, *348*, 122843.
(36) Siegman-Igra, Y.; Reich, P.; Orni-Wasserlauf, R.; Schwartz, D.; Giladi, M. The role of vancomycin in the persistence or recurrence of Staphylococcus aureus bacteraemia. *Scand J. Infect. Dis* **2005**, *37*, 572−578.
(37) Wen, H.; Wu, Q.; Liu, L.; Li, Y.; Sun, T.; Xie, Z. Structural optimization of BODIPY photosensitizers for enhanced photodynamic antibacterial activities. *Biomater. Sci* **2023**, *11* (8), 2870−2876.
(38) Tang, J.; Wang, X.; Chen, S.; Chang, T.; Gu, Y.; Zhang, F.; Hou, J.; Luo, Y.; Li, M.; Huang, J.; Liu, M.; Zhang, L.; Wang, Y.; Shen, X.; Xu, L. Disruption of glucose homeostasis by bacterial infection orchestrates host innate immunity through NAD(+)/NADH balance. *Cell Rep* **2024**, *43* (9), 114648.
(39) Schurig-Briccio, L. A.; Parraga Solorzano, P. K.; Lencina, A. M.; Radin, J. N.; Chen, G. Y.; Sauer, J. D.; Kehl-Fie, T. E.; Gennis, R. B. Role of respiratory NADH oxidation in the regulation of Staphylococcus aureus virulence. *EMBO Rep* **2020**, *21* (5), No. e45832.
(40) Jia, R.; Yang, D.; Xu, D.; Gu, T. Electron transfer mediators accelerated the microbiologically influence corrosion against carbon steel by nitrate reducing Pseudomonas aeruginosa biofilm. *Bioelectrochem* **2017**, *118*, 38−46.
(41) Kim, J.-S.; Liu, L.; Kant, S.; Orlicky, D. J.; Uppalapati, S.; Margolis, A.; Davenport, B. J.; Morrison, T. E.; Matsuda, J.; McClelland, M.; et al. Anaerobic respiration of host-derived methionine sulfoxide protects intracellular *Salmonella* from the phagocyte NADPH oxidase. *Cell Host Microbe* **2024**, *32* (3), 411−424.e10.
(42) Cordero, M.; García-Fernández, J.; Acosta, I. C.; Yepes, A.; Avendano-Ortiz, J.; Lisowski, C.; Oesterreicht, B.; Ohlsen, K.; Lopez-Collazo, E.; Förstner, K. U.; et al. The induction of natural competence adapts staphylococcal metabolism to infection. *Nat. Commun* **2022**, *13* (1), 1525.
(43) Reiß, S.; Pané-Farré, J.; Fuchs, S.; Francois, P.; Liebeke, M.; Schrenzel, J.; Lindequist, U.; Lalk, M.; Wolz, C.; Hecker, M.; Engelmann, S. Global Analysis of the Staphylococcus aureus Response to Mupirocin. *Antimicrob. Agents Chemother* **2012**, *56*, 787−804.
(44) Irving, S. E.; Choudhury, N. R.; Corrigan, R. M. The stringent response and physiological roles of (pp)pGpp in bacteria. *Nat. Rev. Microbiol* **2021**, *19* (4), 256−271.
(45) Anderson, K. L.; Roberts, C.; Disz, T.; Vonstein, V.; Hwang, K.; Overbeek, R.; Olson, P. D.; Projan, S. J.; Dunman, P. M. Characterization of the Staphylococcus aureus Heat Shock, Cold

https://doi.org/10.1021/acsnano.5c06864
ACS Nano XXXX, XXX, XXX−XXX

Shock, Stringent, and SOS Responses and Their Effects on Log-Phase mRNA Turnover. *J. Bacteriol* **2006**, *188* (19), 6739−6756.
(46) Tajbakhsh, G.; Golemi-Kotra, D. The dimerization interface in VraR is essential for induction of the cell wall stress response in Staphylococcus aureus: a potential druggable target. *BMC Microbiol* **2019**, *19* (1), 153.

https://doi.org/10.1021/acsnano.5c06864
ACS Nano XXXX, XXX, XXX−XXX